



# Cosmología y detección del Portal Axión Oscuro
## (Cosmology and detection of the Dark Axion Portal)

**Trabajo de Fin de Máster**
**para acceder al**

**MÁSTER EN FÍSICA DE PARTÍCULAS Y DEL COSMOS**

**Autor: Juan Cortabitarte Gutiérrez**

**Co-Director : Bradley Kavanagh**

**Co-Directora : Núria Castelló Mor**

**Julio - 2021**

# Cosmología y detección del Portal Axión Oscuro (Cosmology and detection of the Dark Axion Portal)

**Resumen**

El Fotón Oscuro y el axión son partículas ligeras y candidatos populares como Materia Oscura, por ser extensiones simples al Modelo Estándar. Cada una de ellas ha sido buscada actívamente a través de sus acoplamientos llamados portal vector y portal axión. El objetivo principal de esta tesis es presentar un modelo (basado en el trabajo de Kunio Kaneta, Hye-Sung Lee y Seokhoon Yun de 2017) que introduce un nuevo portal conectando el Fotón Oscuro y el axión, junto con su fenomenología, implicaciones para la cosmología y detectabilidad. Esto se hará realizando predicciones teóricas acerca de las propiedades del axión y del Fotón Oscuro tal que den cuenta de toda la Materia Oscura, siendo a su vez detectables en experimentos de búsqueda directa. La detectabilidad de los Fotones Oscuros será probada específicamente para la LBC, versión de prueba del experimento DAMIC-M, a través de simulaciones del ruido de fondo y cálculos de la señal esperada de los Fotones Oscuros en el detector de la LBC.

Palabras clave: Materia Oscura, Fotones Oscuros, Axiones, radiopureza, búsqueda directa.

**Abstract**

The Dark Photon and the axion are light particles, popular candidates for Dark Matter for being simple extensions to the Standard Model. Each of them has been actively searched for through the couplings called the vector portal and the axion portal. The focal aim of this thesis is to present a model (based on the work of Kunio Kaneta, Hye-Sung Lee, and Seokhoon Yun in 2017) which introduces a new portal connecting the Dark Photon and the axion, together with its phenomenology, implications for cosmology and detectability. This will be done making theoretical predictions about the properties of the axion and Dark Photon in order for them to account for all Dark Matter while being detectable in direct search experiments. The detectability of Dark Photons will be proven in particular for the LBC, proof-of-concept for DAMIC-M experiment, through simulations of the background noise and calculations of the expected Dark Photon signal in the LBC detector.

Key words: Dark Matter, Dark Photons, axions, radiopurity, direct searches.

# Contents

# 1 Introduction

Dark Matter accounts for 85% of all the matter content in the Universe, however the scientific community still don't know its identity, nor its creation mechanism, nor its interactions. So it remains one of the biggest unsolved problems in physics. Many candidates have been named in the search for Dark Matter but there are only a few well-motivated interactions allowed by Standard Model symmetries that provide a connection (what in the following will be called a "portal") from the Standard Model into Dark Matter [1].

The **Dark Photon** and the **axion** are light particles, popular candidates for Dark Matter for being simple extensions to the Standard Model, and in the case of axions, solving the strong CP problem. Each of them has been actively searched for through the couplings called the vector portal and the axion portal. The focal aim of this thesis is to present a model (based on the work of K. Kaneta, H. S. Lee and S. Yun [2]) which introduces a new portal connecting the Dark Photon and the axion, together with its phenomenology, implications for cosmology and detectability. This Dark Axion Portal allows for new couplings, not just from the vector portal and the axion portal individually. Understanding from the very beginning the development and implications of a particle physics/cosmological model and bringing it to the very end to its experimental detection has been the main goal of work in this thesis, which can be summarized as: i) development of the new Dark Axion Portal model based on [2] and exploration of its implications for cosmology (**Chapter** *2*); ii) exploration of the detectability of Dark Photons for a direct search experiment: the **LBC**, proof-of-concept for **DAMIC-M** (LBC stands for Low-Background Chamber, while DAMIC-M for Dark Matter In CCDs at Modane) (**Chapter** *3*).

## 1.1 Dark Matter

The search for Dark Matter is one of the main research lines among the scientific community, and it has astrophysicists, particle physicists and cosmologists working together. Strong evidence is held on the existence of this form of matter that accounts for approximately 85% of matter on the Universe and 27% of its total energy density [3].

Dark Matter started being investigated in the early twentieth century, with Fritz Zwicky in 1933 applying the virial theorem to infer the gravitational mass of the Coma Cluster, and finding evidence that Dark Matter exists and indeed, in much greater density than luminous matter [4]. This fact started to raise interest for astrophysicists, reaching a peak in the 1960s when Vera Rubin and Kent Ford measured the rotation curve of the Andromeda galaxy leading to new striking evidence on Dark Matter by comparing optical and radio observations [5]. While the optical measurements on galaxies showed a decaying mass distribution from the center, the rotation curves appeared flat, meaning there is some non-visible matter (which density increases towards the outskirts of the galaxy) adding

gravitational force. These two results (clusters and galaxy rotation curves) came together in the 1970s when astrophysicist started to look deeper into cosmology finding both problems were in the end, the same one [6]. This meant a point of no return in Dark Matter investigation, making it one of the main puzzles for modern physics.

Nowadays, there is overwhelming astrophysical and cosmological evidence for Dark Matter as a major constituent of the universe. As mentioned previously, its gravitational influence is necessary to explain why galaxy clusters are bound together [7] and stars move faster than expected around their galaxy [8], the existence of a large-scale structure in the galaxies distribution in the universe [9] and the features in the Cosmic Microwave Background power spectrum [10]. Significant efforts have been made to understand the nature of Dark Matter and theories have been formulated to explain its existence: from Primordial Black Holes [11], to Dark Fluid theory [12], even alternatives such as modified Newtonian dynamics in the Einstein's General Relativity [13], but in general terms, we can not talk about Dark Matter without getting into particle physics, where this work relies.

Despite the success of the Standard Model, Dark Matter is a good reason to believe that there should exist more particles. Many particles have been proposed to solve the Dark Matter problem: some of them related to known Standard Model particles, such as sterile neutrinos [14]; some coming from new symmetries, such as Dark Photons [15]; some that try to explain other problems in particle physics, such as the axion [16] or supersymmetry particles (e.g. gravitino, neutralino...) [17]; and many more with broader properties, such as the WIMPs. WIMPs are Weakly Interacting Massive Particles, i.e. particles which interact via gravity and any other force, which is as weak as or weaker than the weak nuclear force; and have been the main paradigm in the search for Dark Matter in the last years [18]. However, as newer Dark Matter searches have been tightening the net around the WIMP paradigm and they still don't appear, new wider searches are coming in the next few years [19].

Particles that do not interact much with the already known particles are usually known as the dark or hidden sector [20]. Given the complexity of the Standard Model, and knowing it only explains a subdominant component of the Universe, it wouldn't be too surprising if the hidden sector (or sectors, if there were to be more than one) contains a rich structure itself, with Dark Matter making up only a part of it. This hidden sector may contain new light weakly-coupled particles, particles well below the electroweak-scale that interact only feebly with ordinary matter. These feebly interacting particles are the ones that could be detected in direct search experiments.

Particles from the hidden sectors arise in many theoretical extensions to the Standard Model, such as moduli that are present in string theory [21] or new (pseudo-)scalars that appear naturally when symmetries are broken at high energy scales. Other powerful motivations include fine tuning problems, as the strong CP problem, and various experimental findings, including the discrepancy between the calculated and measured anomalous magnetic moment of the muon and puzzling results from astrophysics. Besides gravity, there are only a few well-motivated interactions allowed by Standard Model symmetries that provide a "portal" from the Standard Model into the dark sector [1]. The known portals are shown in *Table 1.1*.

| Portal | Particles | Operator(s) |
|---|---|---|
| Vector | Dark Photon | $-\frac{\epsilon}{2cos\theta_W} B_{\mu\nu} F'^{\mu\nu}$ |
| Axion | Axion (Pseudoscalars) | $\frac{a}{f_a} F_{\mu\nu} F^{\mu\nu}$, ... |
| Higgs | Dark scalars | $\|S\|^2 H^\dagger H$, ... |
| Neutrino | Sterile neutrinos | $LHN$ |

*Table 1.1: Known portals from the Standard Model to the hidden sector. [1]*

In this work our focus will be in the Vector and Axion portal (which will be summarized individually in **Section 1.1.1** and **Section 1.1.2** respectively), specifically in the emergence of a new portal when both are present (what we will call the Dark Axion Portal [2]), which will be put in a cosmological and phenomenological context in **Chapter** *2*. Higgs and neutrino portal are better explored in high-energy colliders and neutrino detectors or astrophysical observations, respectively, which are out of the scope of this thesis.

Unfortunately, no technique (scintillation crystals [22] [23], noble liquids [24] [25] [26], bubble chambers [27], cryogenic calorimeters [28] [29], among others) has been successful yet in the effort to detect directly these theorized particles. Therefore, its nature, so far elusive, constitutes one of the most exciting mysteries in science.

### 1.1.1 Dark Photon

As already mentioned, Dark Matter suggest the possibility of a whole dark (hidden) sector connected feebly with some Standard Model particles, even existing particles of the hidden sector non-interacting with the Standard Model at all. A minimal extension to the Standard Model that allows for this dark sector is the existence of a dark gauge group, that includes an abelian $U(1)$ gauge symmetry. The usual assumption is that the particle associated to such $U(1)_{Dark}$ are heavy, and decouple from the standard model particles, thereby avoiding all observational constraints. But it could be lighter, for example, if the hidden $U(1)$ is broken by non-perturbative effects, the symmetry breaking scale and thus the photon mass is exponentially suppressed, and can be naturally light [15].

Said particle is called Dark (or Hidden) Photon because the dominant coupling to the Standard Model is via kinetic mixing with the Standard Model photon. But what do we mean when we talk about Dark Photon mixing? Similar to neutrino mixing, photons would have two states, and the propagation and the interaction eigenstates would be misaligned. So we have a massless state which couples electromagnetically (photon) and a massive state that doesn't couple to the Standard Model in any other way than via mixing (Dark Photon). Kinetic mixing is allowed by all symmetries, and can be realized via a renormalizable coupling [30]. After a Dark Photon $\gamma\prime$ gets a small mass, the vector portal well below the electroweak scale is given by:

$$\mathcal{L}_{Vector\ \ Portal} = \frac{\chi}{2} F_{\mu\nu} Z'^{\mu\nu}\,, \tag{1.1}$$

where $F_{\mu\nu}$ and $Z'^{\mu\nu}$ are the field strengths of the photon and Dark Photon, $\chi$ is the kinetic

mixing parameter between the two $U(1)$ gauge symmetries ($\chi^2 \ll 1$). The Dark Photon has been motivated from various Dark Matter related physics (such as the positron excess) and other physics (such as the $g_\mu - 2$ anomaly) [2].

This Dark Photon is one of the components in the Dark Axion Portal, and one of the Dark Matter candidates included in the theory of this thesis.

### 1.1.2 Axion

The axion is a particle predicted in 1977 by Robert Peccei and Helen Quinn to solve the strong CP problem in the strong force [31] [32]. Axions have been widely studied both theoretically and experimentally, and there exist many different models for different types of axions. In this subsection we will try to explain a little about how the axions appear, how do they solve (and what is) the strong CP problem and what is their importance as a Dark Matter candidate. To see a further review on the physics of the axion, see [16], [33] or [34].

In very few words, there is no known reasons for the strong force (quantum chromodynamics, QCD) to preserve CP-symmetry (Charge-conjugation Parity symmetry). However, if QCD violated CP-symmetry it should give rise to a measurable neutron dipole moment, which would be comparable to $10^{-18}$ e·m, while the current best measured limit is $(0.0 \pm 1.1) \times 10^{-28}$ e·m [35], meaning that QCD must conserve CP to a very high degree. This is a problem because at the end, there are natural terms in the QCD Lagrangian that are able to break the CP-symmetry. This fine tuning problem is known as the strong CP problem. Many solutions have been proposed to solve this problem, being one of the most important the so-called axion.

In an effective field theory (EFT) description, the Standard Model is extended by introducing a single new pseudo-scalar particle $a$, the axion, for which only one coupling is mandatory, namely an effective coupling to the CP violating topological gluon density $(\frac{a}{f_a} + \theta)G\tilde{G}$, where $f_a$ is the scale suppressing the effective operator, $G = G_{\mu\nu}$ is the gluon field strength tensor, $\tilde{G}_{\mu\nu}$ its dual, and we have added to the axion-gluon operator the CP violating $\theta$ term. With such a simple extension the strong CP problem is solved because the minimum of the vacuum energy occurs when the coefficient of $G\tilde{G}$ vanishes. Thus, by acquiring a suitable vacuum expectation value, the axion disposes of the CP violating operator, therefore acquiring a tiny mass, and appearing as Dark Matter [16]. An important contribution of axions as Cold Dark Matter comes from the misalignment mechanism, explained in **Section 1.2.3**.

Axions thus contribute to Dark Matter, in some theories they account alone for all Dark Matter, but for the theory in this thesis, axions will be the other key particle to fill the Dark Matter density in the Universe, together with the Dark Photon.

## 1.2 Early Universe

To solve some of the already mentioned problems related with Dark Matter, such us the problem with large scale structure and the features in the CMB power spectrum, Dark Matter particles should be created (or exist) in the very early Universe, after inflation, just so their mass density could affect and alter the evolution of the Universe's content.

There are a lot of scenarios that could explain Dark Matter particles appearing in the Early Universe: the inflaton field decaying partly into Dark Matter particles; the latter existing before inflation but in a much greater number density; very feeble interactions that are big enough in the early Universe due to the extreme densities and temperatures creating all the known Dark Matter; or of course, the mixing of all these ideas and many more in some way or the other. This allows for a huge number of theories on many different Dark Matter particles and their possible origin.

In this work we will aim primarily at the idea of a very feeble interaction that could generate the correct amount of Dark Matter in the Early Universe, while maintaining it until the present day. We will have a look at two different mechanisms: **Freeze-Out**, in which the Dark Matter particles are in thermal equilibrium in the Early Universe with the primordial plasma until their interaction with the Standard Model particles is so feeble that it is no longer efficient; **Freeze-In**, which works the other way around, starting with almost no Dark Matter and being created due to a feeble interaction but not entering thermal equilibrium. Many particles, including the Dark Photons, are expected to be created either by Freeze-In or Freeze-Out in many models. We will also explain the **misalignment mechanism**, by which a particle's field oscillates around the potential minimum dissipating energy as particles in the process, the mechanism by which QCD axions are expected to be created.

### 1.2.1 Freeze-Out

In the process of thermal Freeze-Out, Dark Matter particles have a substantial initial density. Particles in the thermal bath are in thermal equilibrium as long as they keep interacting with each other. This condition is met if the interaction rate between particles ($\Gamma$) is higher than the expansion rate of the Universe ($H$). As the Universe evolves, the number density decreases, temperature decreases and the expansion rate of the Universe increases. The idea can be better seen in the scheme in *Figure 1.1*.

At temperatures greater than the mass of the particles, the particle abundance trace its equilibrium value, but when the temperature falls below the mass of the particles, they stop interacting and they reach the relic abundance, i.e. their comoving density *freezes*.

An attractive feature of the Freeze-Out mechanism is that for renormalisable couplings the comoving number density is dominated by low temperatures with Freeze-Out typically occurring at a temperature factor of $20-25$ below the Dark Matter mass, and so is independent of the uncertain early thermal history of the universe eluding possible new interactions at high scales or times like

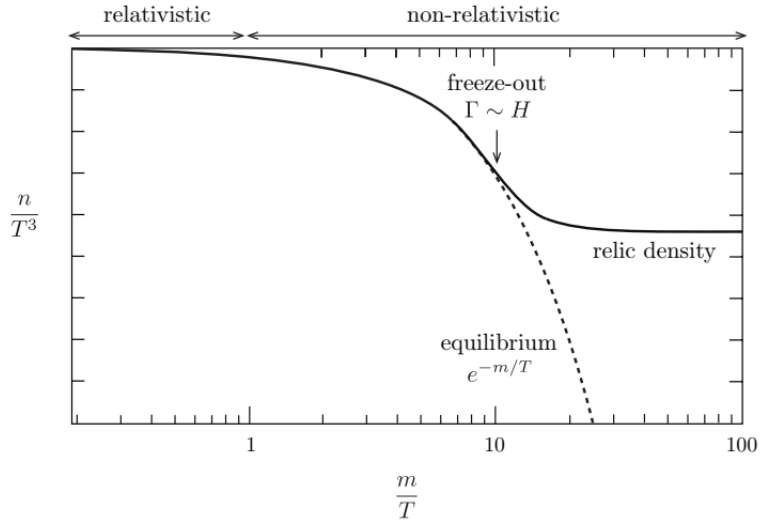


*Figure 1.1: Scheme showing the Freeze-Out mechanism. The dashed line shows the behaviour of the particle number density in equilibrium, but as their interaction is too weak to keep them in thermal equilibrium in an expanding Universe, their relic density freezes [36].*

the Grand Unification. [37]

The Freeze-Out mechanism has been explored a lot in the literature (see for example [36]), being the genesis of many Standard Model particles, such as neutrinos for example, and being the main mechanism explored in the WIMP models.

### 1.2.2 Freeze-In

Freeze-In, as opposed to Freeze-Out, starts with little or no Dark Matter density. Dark Matter particles are created by a feeble interaction, increasing the number density without entering thermal equilibrium. With the expansion of the Universe, the interaction stops being efficient, so the yield becomes fixed. The comparison between Freeze-Out and Freeze-In can be seen in *Figure 1.2*.

Freeze-In has a simple explanation, and because of Dark Matter particles not entering thermal equilibrium, it allows the creation of cold and warm Dark Matter (important for large scale structure) at any mass scale, given that the interaction with the thermal bath is feeble enough.

Dark Matter genesis through this mechanism could happen at very early times in the Universe, allowing for models related with any force, before any phase transition takes place, however it takes us closer to the uncertain early thermal history of the Universe.

Freeze-In mechanism is growing in popularity for new Dark Matter models, such as the one presented in this work. For a detailed explanation on different Freeze-In models and candidates, check [37].

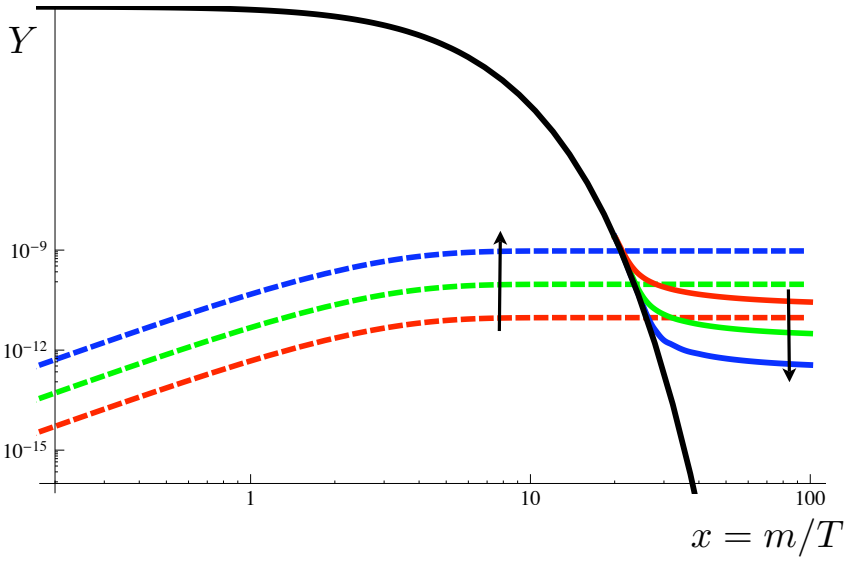


*Figure 1.2: Log-Log plot of the evolution of the relic yields for conventional Freeze-Out (solid coloured) and freeze-in via a Yukawa interaction (dashed coloured) as a function of $x = m/T$ . The black solid line indicates the yield assuming equilibrium is maintained, while the arrows indicate the effect of increasing coupling strength for the two processes. Figure from [37].*

### 1.2.3 Misalignment mechanism

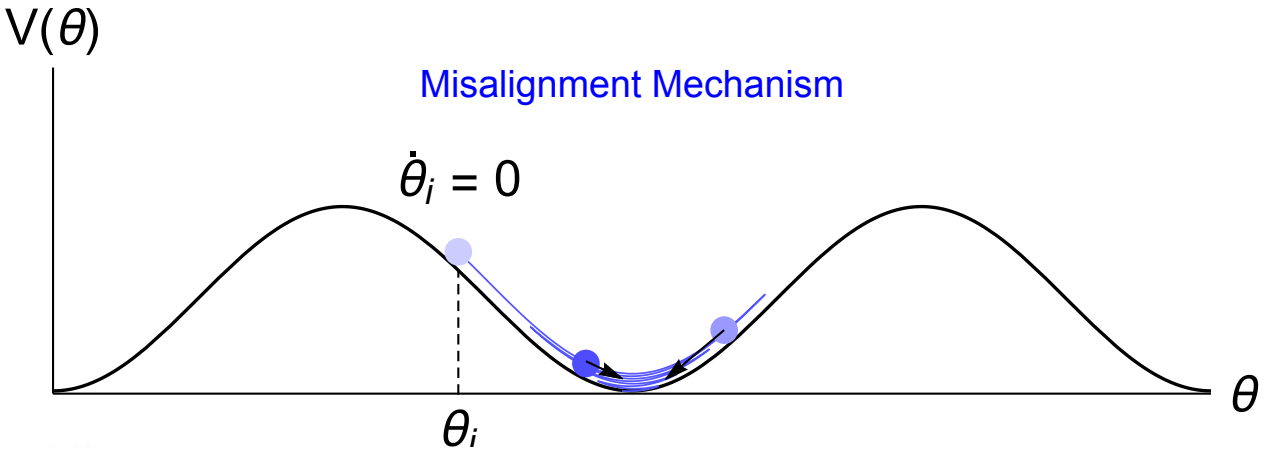


*Figure 1.3: The schematics of the misalignment mechanism. Initial conditions are labeled, shadings from light to dark indicate the time sequence of the motion, and arrows with different relative lengths denote instantaneous velocities. Figure and caption modified from [38].*

Axions can be produced non-thermally (with almost no initial momentum, thus contributing to Cold Dark Matter) through the so-called misalignment mechanism: at the QCD phase transition non-perturbative effects generate a mass for the axion, and the axion field relaxes to the minimum of its potential ($V(\theta)$), which is precisely the Peccei-Quinn (PQ from now on) mechanism, invented to solve the strong CP problem. The oscillation around its minimum (see *Figure 1.3*) produce a coherent state of zero mode axions, i.e. a Bose-Einstein condensate. [39]

The initial value of the axion field potential $\theta_i$ is a free parameter (only if the PQ symmetry is broken after inflation) that fixes the mass scale (and therefore decay constant $f_a$) of the axion. Detailed calculations for the QCD axion and other Axion-Like Particle (ALPs) can be found in [40] or [16].

## 1.3 State of the art in direct detection

A sign of Dark Matter in detectors can be a **direct detection** by observing nuclear or electron recoils from elastic scattering (such as DAMIC [41], XENON [42], DarkSide [43], SuperCDMS [44]), perhaps with the help of an annual modulation as a consequence of the Earth orbit around the Sun (e.g. DAMA/LIBRA [22], ANAIS [45]); or an **indirect detection** by searching for the annihilation products of the Dark Matter being the Dark Matter self-annihilation cross section the constraining factor (e.g. PAMELA [46], FERMI [47]). The vast majority of the experiments are optimized to search for WIMPs (Weakly Interacting Massive Particles) (XENON, DarkSide, LUX/LZ, SuperCDMS, DAMIC), but there are also searches for other Dark Matter candidates: axions (e.g. ADMX [48]), SuperWIMPs (e.g. XENON100 [49], XENON1T [26]), graviton (e.g. CMS [50]), hidden sector (e.g. DAMIC-M [51], LDMX [52]), etc.

Direct detection experiments have been running since 1985, when Goodman and Witten (inspired by the work of Stodolsky and Drukier and their idea of neutrino detection through elastic scattering with nuclei [53]) discussed its usefulness in Dark Matter particles detection [54]. Stodolsky's general idea was to maintain the detector in an unstable equilibrium, so a very little energy injection would make the equilibrium collapse and create an electric signal (via superconductors, scintillators, or semiconductors).

Direct detection searches lay on the broad idea of Dark Matter particles interacting with Standard Model particles feebly, the ones that make up a detector in particular, either by undergoing coherent scattering with nuclei or electrons, or by being absorbed by electrons (important process for Dark Photons and DAMIC-M especially, see [55]).

Different techniques can be used to observe the interaction: either measuring the heat left by the collision (phonon detection via superconductors in cryogenic bolometers like the SuperCDMS), measuring the charge moved by the recoils (ionization in semiconductors, like DAMIC, or bubble chambers like Sensei [56]) or the light emitted by the detector material (scintillators, like DAMA/LIBRA NaI(Tl) crystalls, or ANAIS [45]). Because of these signals being extremely small, some experiments combine two techniques to improve the sensitivity and help with background discrimination as

XENON noble liquid that uses scintillations and ionization or SuperCDMS that uses ionization and heat.

Summarizing, these experiments have been reaching in the past few years many new constraints, like limiting the cross section of the WIMP-nuclei scattering (see left panel in *Figure 1.4*) and the connection between Dark Matter and the electromagnetic force (limiting for example the kinetic mixing parameter between the Dark Photon and the Standard Model photon, see right panel in *Figure 1.4*). This allows for a joint study between phenomenological theoretical work and experimental direct search experiments (where this thesis does its part), with both works playing an important role on constraining the properties and therefore parameter space of Dark Matter particles.

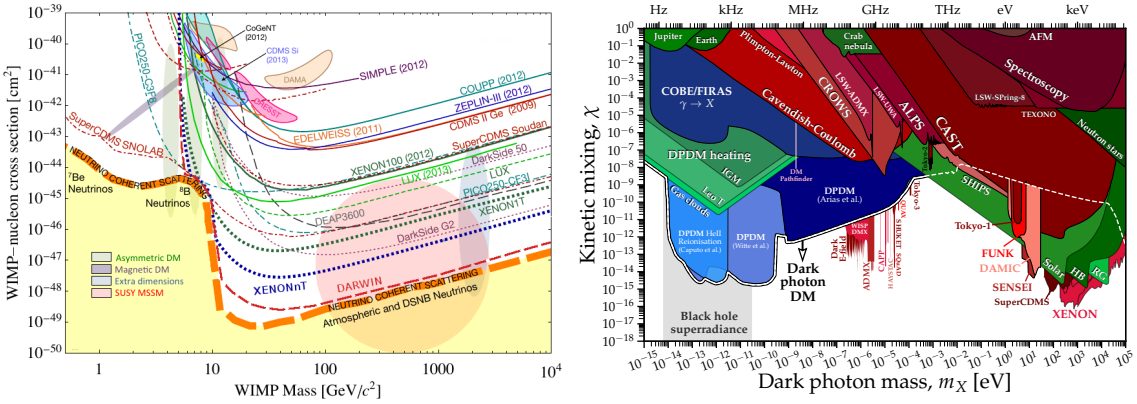


*Figure 1.4: Left: Summary for spin-independent WIMP-nucleon scattering results. At very low cross sections ($\sim 10^{-50}$ $cm^2$) the neutrino background (yellow region) will start to dominate the recoil spectrum. Figure taken from [57]. Right: Current constraints on the Dark Photon's mass, $m_X$, and kinetic mixing parameter with the Standard Model photon, $\chi$. The general colour scheme is: cosmological bounds in blue, experimental bounds in red (in which appear many of the already mentioned direct search experiments), and astrophysical bounds in green. Figure taken from [58].*

In order to find these low energy recoils, Dark Matter direct detection experiments need a low energy threshold and a very low background (or at least, to be able to discriminate already known background). This is mandatory to be able to detect the low-energy nuclear recoils or electron ionization along with a small rate event, thus there is also a need for large detector mass and long term stability, in order to collect as much data as possible at once, reducing exposure time.

It is important to recognize that current experiments have limited sensitivity to Dark Matter-electron interactions, and a light Dark Matter particle may have well escaped detection. Most of the interactions result in the production of few charges, requiring the detector to be able to resolve individual electrons. A challenge for direct search experiments is also to differentiate sources of background (natural radioactivity, airborne radon, neutrons, $\alpha$ particles, neutrinos, etc.) which must be really low for a signal to be recognizable. In the case of semiconductor or photosensitive devices, a low dark current (charges generated in the detector when no outside radiation is entering the

detector like spontaneous creation of electron holes due to thermal energy, defects on the crystalline structure of the semiconductors, etc) is also a prerequisite to building a detector to search for light Dark Matter using Dark Matter-electron interactions so the electrons ripped away by Dark Matter interactions are not mistaken for thermal noise.

It is worth mentioning how all this direct searches focus on the search of massive particles with feeble interactions (an extension to the WIMP paradigm), while there are a lot of experiments searching for well motivated Dark Matter candidates that can not be detected like this and have their own experimental methodologies in order to search for them, such as searches for sterile neutrinos [59] or axions. Axion searches are closely related with this work and are an important part of its raison d'être (being able to have a model that accounts for all Dark Matter and is also detectable), but it is a vast field with many different experimental approaches and the implication with the experimental search for the axion is out of the scope of this thesis. To see a review on axions and axion-like-particles (ALPs) searches, see [60].

### 1.3.1 DAMIC-M and the use of CCDs as a Dark Matter detector

As already mentioned, the scope of this work is the upcoming DAMIC-M Experiment, the upgrade of DAMIC, and especially its proof of concept the Low Background Chamber or LBC. DAMIC used CCDs (charged coupled devices) made of silicon to find signals in the detectors different from the noise when interacting with $Si$ atoms.

DAMIC-M CCDs are fabricated from n-type, high-resistivity silicon wafers and they feature a three-phase polysilicon gate structure with a buried p-channel [61]. Each CCD is fully depleted by applying a potential $\geq$ 40 V to a thin back-side contact. The detection process with CCDs starts with the charge produced due to the interaction between the ionizing particle and the silicon bulk, being drifted towards the pixel gates, where it is stored in potential wells until the readout. After a given exposure time, the readout process starts and the charge is transferred vertically from pixel to pixel along each column until it reaches the last row, the so-called serial register. The signal is based essentially on i) ionization signals produced by the interaction of Standard Model particles with the silicon bulk of the CCDs (background noise), ii) the intrinsic detector noise composed of the dark current and electronic noise (during readout time) and iii) (if found) the Dark Matter signals, through absorption or nuclear/electronic recoil [51]. In other words, these signals from ionizing particles, known as tracks, are energy deposited in silicon pixels along the particle trajectory within the silicon bulk of the CCD.

One of the greatest feats for the DAMIC experiment was achieving the lowest dark current ever measured in a silicon detector: 4 $e^-/mm^2/day$, allowing Dark Matter detection over 10 eV, which will be carried to DAMIC-M experiment. This energy regime is very important for Dark Photon absorption in electrons [62, 63], as will be explored in **Chapter** *3*.

Following the great results from DAMIC experiment comes DAMIC-M (which stands for DAMIC at Modane), the next generation of the DAMIC detector. DAMIC-M, with the most massive ever built CCDs: 1-kg detector made of 200 CCDs, each of them with a mass of about 5 g. Every

CCD will feature 6k x 1.5k pixels over a 9 cm x 2.25 cm area and a thickness of at least 0.675 mm. DAMIC-M will be installed in 2023 at the *Laboratoire Souterrain de Modane* in France, located 1700 meters below Fréjus peak. These are the most massive ever built CCDs, with an improvement made by the Lawrence Berkeley National Laboratory: the “skipper" amplifier [64]. The skipper amplifiers measure the charge collected by each CCD pixel several uncorrelated times, decreasing the pixel noise by averaging over a large number of samples, as the readout noise goes as $\frac{1}{\sqrt{N}}$, with $N$ the number of times you read the charge of one pixel. The readout noise achieved with 4000 samples is 0.068 electrons (0.26 eV) [65]. This makes the readout noise negligible and therefore makes dark current the limiting noise.

The detector design is still under development. The baseline scheme is shown in *Figure 1.5* (left). A cryostat vessel will house the CCDs, packed in a box surrounded by different shieldings (Lead and polyethylene). Cooling will be provided by the use of liquid nitrogen, whose consumption will be optimized by a heat exchanger. Most of the components will be made of electro-formed (EF) copper, especially those nearest the CCDs, given their very low content of radioactive isotopes, while farther volumes will instead be made of oxygen-free high thermal conductivity (OFHC) copper. In the simple configuration similar to DAMIC's one, CCDs are disposed horizontally, on the top of each other (*Figure 1.5*, right (a)). Each CCD is hold in a EF copper frame which ensure mechanical support for the CCD and cables and thermal contact.

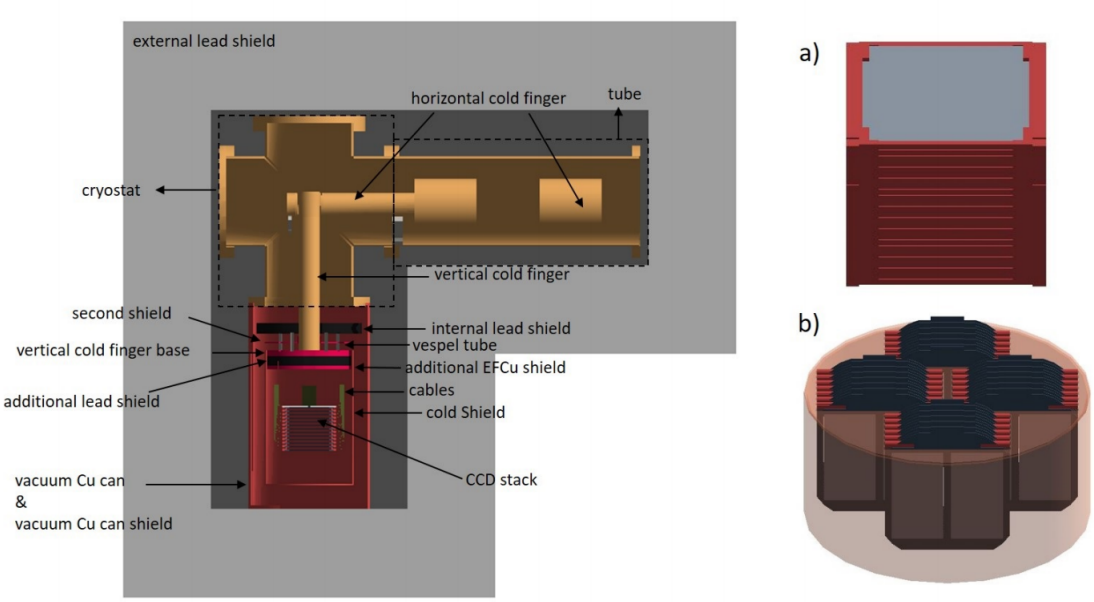


*Figure 1.5: Left: latest simulated detector design. The electro-formed copper components are shown in red, while the OFHC copper ones in yellow. Right: zoom on two possible solutions for the CCD stack. a) Horizontal CCD stack. b) Vertical CCD stack. The gray parts are the CCDs, the red parts the copper holders.*

When compared to other Dark Matter detector types, CCDs present some unique properties, that allows to reach very low masses, particularly in models which imply electron scattering or absorption where CCD Dark Matter detectors expect to have very good sensitivities. The crucial innovations in the DAMIC-M CCD detector are:

1. Unprecedented single-electron resolution by including *skipper readout*: 0.1 for $<$ 1rms pixel readout time. R&D lead by Fermilab within the SENSEI group is already underway.
2. Extremely low leakage current (intrinsic detector noise) will be achieved by including IR shields (layers of polyethylene and Lead surrounding the detector) and by operating the skipper CCDs at low temperatures.
3. Exquisite spatial resolution and 3D reconstruction, simulations show the ability to eliminate backgrounds (such as the intrinsic $^{32}$Si: a radioisotope that appears from the silicon in the CCDs, meaning all its noise is automatically detected due to being inside the CCD itself) by rejecting pairs of events consisting with the same origin.

Given the great noise reduction expected in the DAMIC-M CCDs, the last challenge to the detection process is the background noise, which could obscure the Dark Matter detection. Some of the main background sources are:

- the environmental radioactivity including airborne radon and its daughters.
- radio-impurities in the detector construction and shield material.
- neutrons from $(\alpha, n)$ and fission reactions.
- cosmic rays and their secondaries.
- activation of detector materials during exposure at the Earth's surface.

A careful study of the radioactive background in order to decrease it below 0.1 keV/kg/day is needed for the Dark Matter direct detection. This is done through improvements in the experiment design, the selection of the construction materials and through radioisotopes simulations for the background study. Environmental radioactivity is controlled in the facility with a good ventilation system to avoid radon, along with the shielding for the CCDs.

In this work, the detectability was explored by making background simulations using the Low Background Chamber (LBC from now on) which is an experiment at Modane, delayed because of the COVID-19 pandemic, to test the CCD readout and other features for DAMIC-M (data taken, electronics, etc) with 2 CCDs like the ones that will be used for DAMIC-M. Other important goal for LBC is to test the background models and do some science as with the new skipper CCDs the detection limits are expected to be lower than those of DAMIC.

As the Low background chamber design is finished (the chamber will start working at the end of this year), this work will be concentrated in the study of the background noise in this prototype. Once the DAMIC-M design is done completely, this work could be extended to the full experiment, as the external experimental setup will be similar in both cases, and also similar to that of DAMIC.

## 1.4 Aim of this study

This work is meant to present a Dark Matter direct search experiment in all its aspects, from evaluating a particle physics model and its implications for cosmology, to probing its detectability in a detector. In order to do that a model mixing axions and Dark Photons (two well motivated candidates for Dark Matter) known as the *Dark Axion Portal* has been studied. All its theoretical background along with its implications for cosmology will be explained and calculated in **Chapter** *2*.

As the final part of the modelling its detectability has been calculated (cross-section, event rate, recoil energy...) for a direct search experiment, in particular, LBC. In order to probe said detectability, simulations of the background noise on the LBC (proof-of-concept of DAMIC-M) experiment have been done using two different pieces of software: DAMICG4 and psimulCCDimg. A better explanation will be given in **Chapter** *3*.

This allows to study the background noise coming from radioisotopes and compare it to the event rate of the studied model, checking if the detection of, in this case, the Dark Photon is possible. The detection of axions is out of the scope of this work, although the axion search is a very active experimental field.

The study of the Dark Photon detection allows to predict the detection limits of both the LBC and DAMIC-M, which will be presented in **Chapter** *4*.

# 2 | Dark Axion Portal Cosmology

The theoretical model presented in this thesis relies on the work of Kunio Kaneta, Hye-Sung Lee, and Seokhoon Yun [2] and their idea of the Dark Axion Portal. In this section we will present the theoretical background and give a general idea of what the Dark Axion Portal is.

The Dark Axion Portal connects the axion and the Dark Photon (two well motivated Dark Matter particles, as already explained in **Section 1.1.2** and **Section 1.1.1** respectively). In the presence of the Dark Photon, an axion can couple to two photons, two Dark Photons as well as a photon and a Dark Photon. These interactions are given by the nonrenormalizable Dark Axion Portal terms:

$$\mathcal{L}_{Dark\ \ Axion\ \ Portal} = \frac{G_{a\gamma\prime\gamma\prime}}{4} a Z'_{\mu\nu} \tilde{Z}'^{\mu\nu} + \frac{G_{a\gamma\gamma\prime}}{2} a F_{\mu\nu} \tilde{Z}'^{\mu\nu} \,. \tag{2.1}$$

These couplings are shown in *Figure 2.1*. For our theory we will always be talking about KSVZ axions (for the details of this axion model see [66, 67]), for them to solve the strong CP problem apart from being Dark Matter. The Dark Axion Portal could also be valid using ALPs and changing axions parameters, but we will stick to the QCD axion, KSVZ model in particular to keep it as simple, minimal extension to the Standard Model (a review of the KSVZ axion together with other axion models can be found at [16]).

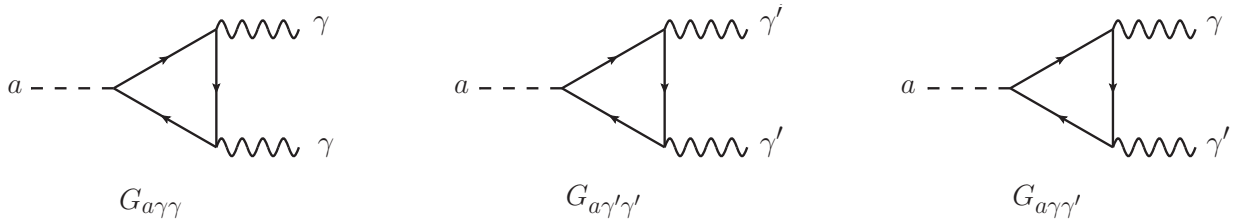


*Figure 2.1: Axion-Dark Photon Coupling. Note the fermions in the triangle loop can have both $U(1)_{PQ}$ and $U(1)_{Dark}$ charges as well as the electromagnetic charges, and the Dark Photon can couple to them directly. Figure from [2]*

The couplings are given by:

$$G_{agg} = \frac{g_S^2}{8\pi^2} \frac{PQ_\Phi}{f_a} \,, \tag{2.2}$$

$$G_{a\gamma\gamma} = \frac{e^2}{8\pi^2} \frac{PQ_\Phi}{f_a} \left( 2N_C Q_\psi^2 - \frac{2}{3} \frac{4+z}{1+z} \right) \,, \tag{2.3}$$

$$G_{a\gamma\gamma'} \simeq \frac{ee'}{8\pi^2}\frac{PQ_\Phi}{f_a}\left(2N_C D_\psi Q_\psi\right) + \chi G_{a\gamma\gamma}\,, \tag{2.4}$$

$$G_{a_{\gamma'}\gamma'} \simeq \frac{e'^2}{8\pi^2}\frac{PQ_\Phi}{f_a}\left(2N_C D_\psi^2\right) + 2\chi G_{a\gamma\gamma'}\,, \tag{2.5}$$

where $e$ is the electromagnetic coupling, $N_C = 3$ is the color factor, $z = m_u/m_d \simeq 0.56$ is the ratio between the mass of the up and down quark, $g_S$ is the $SU(3)_C$ coupling (related with the strong force coupling constant as $\alpha_S = \frac{g_S^2}{4\pi} \simeq 0.12$ at high energies), $e'$ is the $U(1)_{Dark}$ coupling (which can be as sizable as the Standard Model gauge couplings), $\chi$ is the kinetic mixing parameter of the Dark Photon, $D_\psi$ is the $U(1)_{Dark}$ charge of the axion, $PQ_\Phi$ the $U(1)_{PQ}$ charge, and $Q_\psi$ the electromagnetic anomaly of the axion.

As $e'$ can be as sizable as the Standard Model gauge couplings, it can be seen from these expressions how the Dark Axion Portal creates new relatively large couplings from the dark gauge symmetry (it could be as large as the axion coupling to the Standard Model photons), even when the connection with the axion-photon-photon coupling is greatly suppressed ($\chi^2 \ll 1$).

Axions have electromagnetic and color anomaly to make them more interactive with photons and gluons respectively. These anomalies are model-dependent, so in our case, to keep things simple we will tune the electromagnetic anomaly $Q_\psi$ to 0, so that axions interaction with photons is minimized. All in all, our general charge assignment will be $PQ_\Phi = 1$, $e' = 0.1$, $D_\psi = 3$ and $Q_\psi = 0$.

The model can get quite complicated and have multiple extensions if the parameters are changed, therefore we will use a careful approach to unveil the cosmological implications of this model step by step as it follows:

- First, in **Section 2.1**, we analyze the model with the couplings mentioned before assuming there is no kinetic mixing between the Dark Photon and the Standard Model photon, i.e. $\chi = 0$.
- Then, in **Section 2.2**, we will forget for a while about the Dark Axion Portal and we will calculate the cosmological implications of just having Dark Photons kinetically mixed with the Standard Model photons.
- Finally, in **Section 2.3**, we will merge both approaches and see how the Dark Axion Portal behaves with Dark Photons being kinetically mixed with Standard Model photons, and we will be able to check if the final model is detectable while accounting for all Dark Matter in the Universe summing the axions and Dark Photons contributions (this will be left for **Chapter** *3*).

## 2.1 Axions create Dark Photons

As an starting point to this theory we have production of Dark Photons through Freeze-In mechanism. The interaction leading the Freeze-In is gluon annihilation, with the axion mediating the interaction. The Feynman diagram of the interaction is:

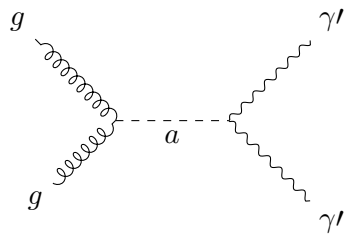


*Figure 2.2: Gluon annihilation to Dark Photon pair production mediated by the axion.*

This annihilation happens at very early times in the Universe, right after inflation, so that the temperature and density of the primordial plasma is large enough to allow this interaction.

One can relate the density parameter of Dark Photons with the properties of the axion and the Dark Photon as in equation 17 in [2]:

$$\Omega_{\gamma'}h^2 \approx \frac{S_0 m_{\gamma'} 1080\sqrt{10}\alpha_s^2 P Q_\Phi^4 e'^4 D_\psi^4 36 M_{Pl} T_{RH}^3}{256\rho_c g^{3/2}\pi^{15} f_a^4}\,, \tag{2.6}$$

where $S_0 = 2889.2$ cm$^{-3}$ is the entropy density at the present time, $\rho_c = 1.05368 \times 10^{-5}$GeV cm$^{-3}$ the critical density, $M_{Pl} \approx 2.4 \times 10^{18}$ GeV the Planck Mass, $\Omega_{\gamma'}h^2$ the density parameter (0.12 to take account for all the Dark Matter in the Universe), $g = 100$ the number of degrees of freedom of the thermal bath of the Universe during the creation of the Dark Photons, $\alpha_s = 0.12$ the strong coupling constant, $T_{RH}$ the reheating temperature of the universe (temperature at which the Universe is at the end of inflation) and $m_{\gamma'}$ the mass of the Dark Photon.

The calculations that lead to this equation are long, and in general do not provide vital information for the reading of the thesis. They are left out of the main body of this thesis but can be found in Appendix *A*, from obtaining the entropy density in the Early Universe, passing through the development of the Boltzmann equation for Dark Photons density, to the Equation (2.6) here presented.

So this equation relates the mass of the Dark Photon with the axion decay constant and therefore to the mass of the axion, because after the QCD phase transition, the axion mass is given by:

$$m_a \simeq \left[\frac{\sqrt{z}}{1+z}\right]\frac{f_\pi}{f_a} m_\pi\,, \tag{2.7}$$

where $z = \frac{m_u}{m_d} \simeq 0.56$, and $m_\pi \simeq 135$ MeV and $f_\pi \simeq 92$ MeV are the mass and the decay constant of the pion, respectively, giving $m_a \approx \frac{5957.87\ \text{MeV}^2}{f_a}$.

Therefore, from eq. (2.6) we can get a plot for the mass of the axion in terms of the mass of the Dark Photon if we fix the Dark Matter relic abundance to fit all the Dark Matter in the Universe ($\Omega_{\gamma'}h^2 = 0.12$), for given values of the reheating temperature (as we have chosen the dark portal interaction charges), as illustrated in *Figure 2.3*, matching the plot in [2].

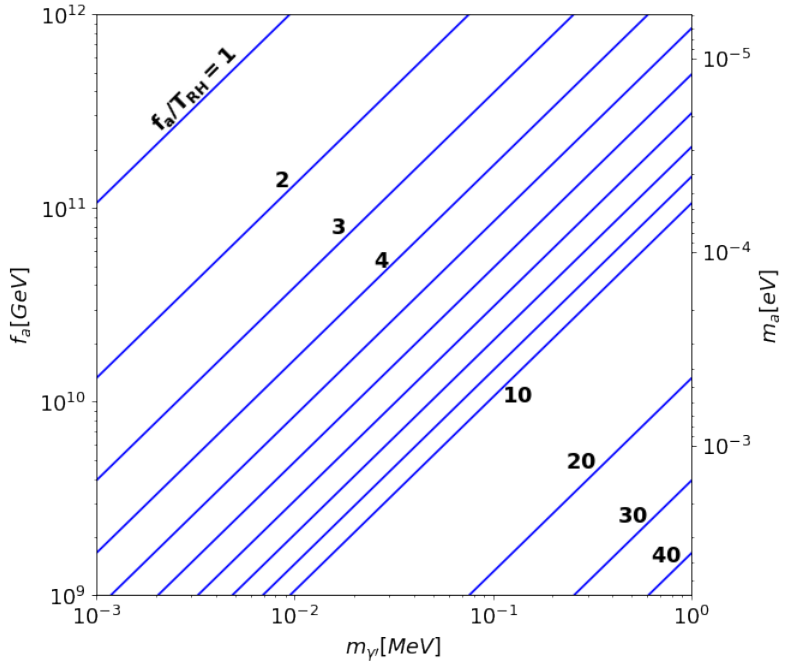


*Figure 2.3: The blue lines show* $\Omega_{\gamma'}h^2 = 0.12$ *for the given* $f_a/T_{RH}$ *values. We choose* $e' = 0.1$, $D_\psi = 3$, $PQ_\Phi = 1$ *with* $g = 100$. *For low* $f_a$ *, the axion alone cannot explain the observed relic density, yet it can be accounted for with the Dark Photon.*

*Figure 2.3* shows the linear correlation between the mass of the axion and the mass of the Dark Photon, for any value of the reheating temperature.

For it to be more understandable, we set the solid lines to be only $T_{RH}$ dependent instead of the $f_a/T_{RH}$ ratio, we extend the plot limits, and we set some known constrains. These constrains are:

- Upper bound on $m_a$: Peccei-Quinn axions cannot be heavier than $\approx 10^{-3}$ GeV due to Supernova observations [33]
- Lower bound on $m_a$: They can't also have a mass lower than $\approx 10^{-5}$ GeV, because due to the misalignment mechanism, that would lead to a higher density parameter than the one for all Dark Matter in the Universe (0.12) [68].
- Lower bound on $T_{RH}$: The reheating temperature "must be" higher than $10^9$ GeV due to leptogenesis [69].
- Lower bound on $m_{\gamma'}$: If you want to use the Freeze-in mechanism, you need to avoid entering thermal equilibrium. This sets an upper constrain in the reheating temperature, because if the temperature is too high the Dark Matter annihilation takes place most frequently and it might be thermalized. Once entered this constraint in (2.6), it forces a lower bound on the mass of the Dark Photon (for $\Omega_{\gamma'}h^2 = 0.12$ that is $m_{\gamma'} > 157$ eV, however for smaller values

of $\Omega_{\gamma\prime}h^2$ the constraint relaxes and Dark Photon mass can be lowered, see Appendix $B$ for the detailed calculation). This is an important constraint for Freeze-In model, not remarked by [2], that sets very valuable experimental boundaries.

With the constraints and the same conditions as in the first figure (*Figure 2.3*) we can plot *Figure 2.4*.

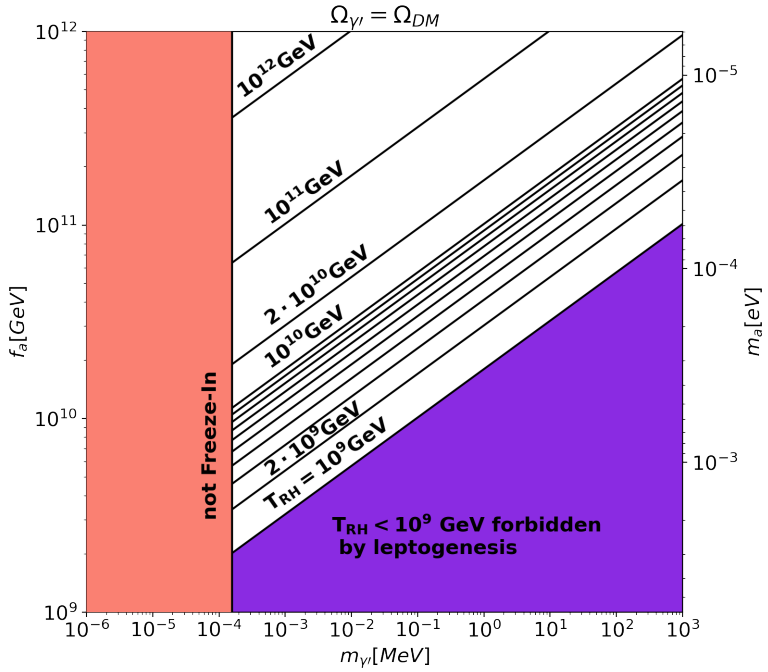


*Figure 2.4: Figure 2.3 with the same parameters but putting the lines as a function of only the $T_{RH}$ and setting the mentioned constrains.*

Once we have the results for the Freeze-In model, we can try to fit in this parameter space the Freeze-Out model, which should give permitted values (if any) out of the boundaries of the Freeze-In model.

After performing the calculations (check Appendix $C$ for more information), the relativistic Freeze-Out model shows a single value for the Dark Photon mass (which is 1/3 of the lower limit in the Freeze-In). This is because the Dark Photons are in thermal equilibrium while being highly relativistic in the Freeze-Out model, when $T \gg m_{\gamma\prime}$, and the Yield becomes fixed from that moment on, fixing the mass and not depending on the axion parameters. The non-relativistic Freeze-Out model gives a single line of values, dependent on $f_a$ and the density parameter $\Omega_{\gamma\prime}h^2$. This is shown in *Figure 2.5*.

The other change between *Figure 2.4* and *Figure 2.5* is the inclusion of the axion relic density to check if it is truly negligible.

As in this model we work with the QCD axion, some of its properties have been well explored. One is the axion contribution to the Universe's energy density, done by Fox, Pierce and Thomas in [68] and quoted by Peccei in [33]:

$$\Omega_a h^2 = 0.5 \left[\frac{f_a/\xi}{10^{12}\ \text{GeV}}\right]^{\frac{7}{6}} \left[\theta_i^2 + \sigma_\theta^2\right] \gamma\,, \tag{2.8}$$

where $\xi$ is the coefficient of the Peccei-Quinn anomaly ($\xi = 1$ for KSVZ models, the one we are using), $\gamma$ is the dilution factor (we assume no dilution, so $\gamma = 1$), $\theta_i$ the misalignment angle (average is $\left\langle \theta_i^2 \right\rangle = \frac{\pi^2}{3}$) and $\sigma_\theta$ its fluctuations (we neglect them, so $\sigma_\theta = 0$).

This gives a constraint for the maximum value of $f_a$ (or what is the same: a minimum value for $m_a$), for $\Omega_a h^2 = 0.12$ if we only had axions as Dark Matter, but in our case, we also have Dark Photons. Then the constraint builds up as $\Omega_{\gamma'} h^2 + \Omega_a h^2 = 0.12$, and then both components have to share the parameter space. It can be seen how if we make the axion density parameter negligible, let's say 0.001, then $f_a = 1.75 \times 10^9$, and thus it cannot fit into the parameter space, as it is forbidden by the lower bound on the reheating temperature. This forces us to take both density parameters into account, which is shown in *Figure 2.5*.

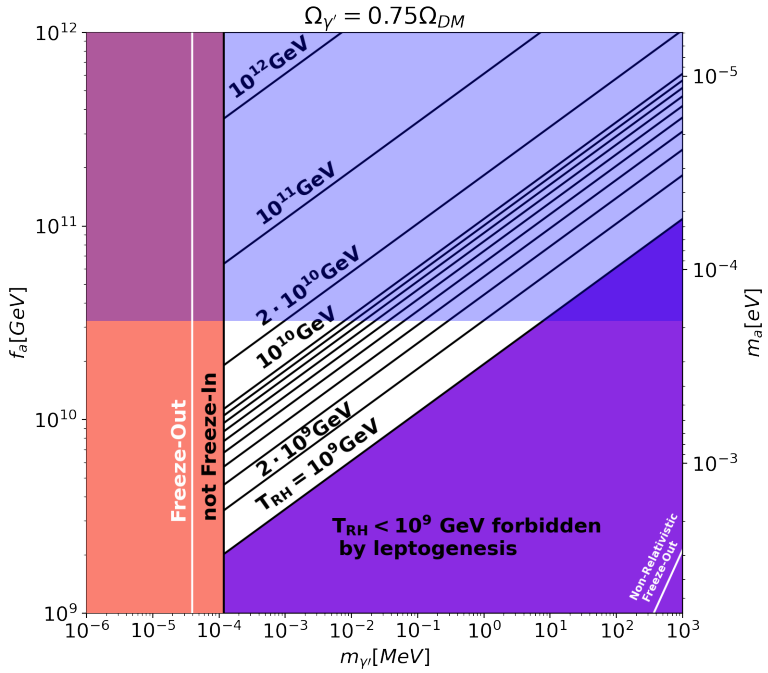


*Figure 2.5: Figure 2.4 including a constrain in the axion mass for its density parameter (in this case as exempli gratia $\Omega_{\gamma'} h^2 = 0.09$, $\Omega_a h^2 = 0.03$ assuming all DM is axions + Dark Photons) in blue, and the Freeze-Out mass of the Dark Photon.*

It is important to remark how the shaded blue region in *Figure 2.5* corresponds to example

values of the importance of the axion density parameter. It constraints even more the parameter space when taken into account, and it is not negligible. Only when the density parameter of the axion is large is the parameter space open, as the shaded region goes up (the mass of the axion can be smaller) and the minimum value for the Dark Photon mass because of Freeze-In gets reduced (so the mass of the Dark Photon can also be smaller). If the amount of axions as Dark Matter in the Universe is small, then the mass of the Dark Photon is strongly constrained.

Now we can do some little approximations to see how easily can we detect this Dark Photons that couple to the Standard Model just through the axion.

In order to try and direct detect this Dark Photons, we have to do at least a sloppy approximation to see the order of magnitude of: a) the recoil energy in the detector and b) the cross section of the interaction. With these two we can have an idea on how well will the direct detection be. For these calculations we will use DAMIC-M experiment as an approach, which uses silicon CCDs as detectors. Therefore we will calculate the energy recoil of silicon nuclei when scattering a Dark Photon, and we will check the cross section of a Dark Photon scattering with a gluon in said nuclei.

Taken that the Dark Photons now have a relative velocity of $\sim$ 100 km/s (dispersion velocity in the Milky Way) the elastic scattering occurs in the extreme non-relativistic limit, and the recoil energy of the nucleon is easily calculated in terms of the scattering angle in the center of mass frame $\theta^*$ [70]:

$$E_R = \frac{\mu_N^2 v^2 (1 - cos\theta^*)}{m_N}\,, \tag{2.9}$$

where $\mu_N = \frac{m_{\gamma\prime} m_N}{m_{\gamma\prime} + m_N}$, the DP-Nucleus reduced mass. The recoil energy must be smaller than the scattering with the best conditions, i.e. opposite velocities for Earth and the Dark Photon, so $v \sim 200$ km/s $\sim 6.67 \times 10^{-4}$ c; perfect $180^\circ$ scattering angle. Knowing the mass of a silicon nucleus $m_N \approx 2.63 \times 10^{10}$ eV, and assuming a heavy Dark Photon $m_{\gamma\prime} = 1$ GeV:

$$E_R \lesssim 32 \text{ eV}\,. \tag{2.10}$$

And this approximation is for a very heavy Dark Photon (almost out of the parameter space of *Figure 2.5*) and without taking into account the efficiency of the detector to transform the energy recoil into a readable current. Due to the axion having a very little mass, there are corrections that would enhance the energy recoil, but very littly, so the direct detection within this model seems very hard, as typically CCD detectors have a threshold of a few tens eV.

To calculate the cross section we can use the Feynman diagram of the interaction:

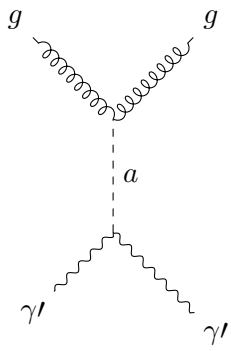


*Figure 2.6: Dark Photon gluon scattering mediated through the axion.*

The upper vertex will have $G_{agg}$ eq. (2.2) as coupling, while the bottom one will be $G_{a\gamma\prime\gamma\prime}$ eq. (2.5), so its cross section can be approximated as:

$$\sigma v \sim \frac{1}{s}|G_{agg}q^2\frac{1}{q^2}G_{a\gamma\prime\gamma\prime}q^2|^2 \sim G_{agg}^2 G_{a\gamma\prime\gamma\prime}^2\frac{t^2}{s}\,, \tag{2.11}$$

as q, the four-momentum of the exchanged particle is $q \sim \sqrt{t}$, the energy in the center of mass reference frame.

As all the initial momentum of the Dark Photon ($p_2$) is transferred to the gluon ($p_3$), which has 0 initial momentum ($p_1 = 0$), and remembering the Mandelstam variables ($s = (p_1 + p_2)^2$ and $t = (p_1 - p_3)^2$) we have:

$$\sigma v \sim G_{agg}^2 G_{a\gamma\prime\gamma\prime}^2\frac{t^2}{s} \sim G_{agg}^2 G_{a\gamma\prime\gamma\prime}^2\frac{(-p_2)^4}{(p_2)^2} \sim G_{agg}^2 G_{a\gamma\prime\gamma\prime}^2 p_2^2\,. \tag{2.12}$$

If we take $p_2 = m_{\gamma\prime}v_{\gamma\prime}$, where $v \sim 100$ km/s and $m_{\gamma\prime} = 1$ GeV, and we take a reasonable value for $f_a$ such as $10^{11}$ GeV, then we find:

$$\sigma v \sim 1.9 \times 10^{-77}\ \text{eV}^{-2} \sim 7.4 \times 10^{-87}\ \text{cm}^2\,. \tag{2.13}$$

This is a terrible result, not only because it is almost 50 orders of magnitude below any modern direct search experiment for that mass, but because it is even 40 remarkable orders of magnitude below the neutrino floor, cross section sensitivity at which the neutrinos would be detected in the same way as Dark Matter. Corrections on spin-dependent scattering are more important in this case than in the case of energy recoil calculations, however they won't cover the 50 orders of magnitude that separate the theory from the experiments.

So with this calculations it is demonstrated that an experiment like DAMIC-M wouldn't be enough to detect this Dark Photons, and no experiment would be capable in the early future.

At this point we will put a halt in the gluon-gluon-axion to axion-DP-DP model to focus on the

kinetic mixing between Dark Photons and Standard Model Photons. Later we will come back to mix both models into one and see the improvements in direct detection.

## 2.2 Standard Model photons create Dark Photons

We now seek enlightenment in a new paper [15]. From this paper we can obtain the Yield equation for this new process (what we are looking for) and new constraints for the model, but we will do it slowly anyway.

Dark Photon mixing, as explained in **Section 1.1.1**, gives a massless state which couples electromagnetically (photon) and a massive state that doesn't couple to the Standard Model in any other way than via mixing (Dark Photon). Therefore we will denote $\gamma$ and $\gamma\prime$ the flavor states, while $\gamma_1$ will be mostly a "photon-like" mass eigenstate and $\gamma_2$ the "Dark Photon-like". This mixing leads to photon oscillations in vacuum, with a tiny mixing angle (i.e. a tiny probability of oscillation), however we are interested in the oscillation in the Early Universe, which should be greater to account for all the Dark Matter in the Universe today.

In the Early Universe, the photons were in a thermal plasma, so matter effects should be taken into account. We can include the influence of the plasma in the photon propagation through the photon's self energy, which acts a complex effective mass denoted by $\omega D$. The real part of the mass encodes the refraction properties of the plasma and we will refer to it as the plasma mass or the photon mass denoted by $m_\gamma$. The relevant definitions and calculations on the effective mass of photons in a plasma can be found on [15], for now we will just keep for ourselves the idea that in a plasma, the photons gain an effective mass that allows a resonance whenever the effective mass of the photons matches the mass of the Dark Photons, allowing a peak in Dark Photon production. This can be seen especially in the expression for the effective mixing angle in a damping dominated medium, given by [71]:

$$\chi^2(\omega, T) \simeq \chi_0^2 \frac{m_{\gamma\prime}^4}{\left(m_{\gamma\prime}^2 - m_\gamma^2\right)^2 + (\omega D)^2}\,, \tag{2.14}$$

where $\chi_0$ is the kinetic mixing parameter in vacuum. This expression shows how the effective mixing angle depends implicitly on the energy and the temperature through $m_\gamma$ and $\omega D$. The imaginary contribution to the photon mass, $\omega D$, is typically smaller than the real part, $m_\gamma$, so it only plays a role near the resonance $m_\gamma = m_{\gamma\prime}$ where it acts as a cut off.

There are several important mass regimes with different production mechanism. Whether the mass of the Dark Photon is greater than two times the mass of the electron is important, as it would lead to pair production of Dark Photons in electron-positron annihilation. In this work we will just focus in the idea of light Dark Photons $m_{\gamma\prime} < 1$ MeV, so the production mechanism relevant to us is resonant production. Electrons are non-relativistic for such light Dark Photons, thus $m_\gamma \propto T^{3/2} e^{-m_e/T}$, so in the range 1 eV$< m_{\gamma\prime} < 1$ MeV the resonance happens not far from

$T_r \sim 0.2 m_e$.

At high temperatures for which $m_\gamma(T) \gg m_{\gamma\prime}$ the hidden photon is comparatively massless; photons are very close to being both interaction and propagation eigenstates and the effective mixing angle is strongly suppressed. Consequently the amount of hidden photons produced is negligible small. We can therefore assume that the initial abundance of hidden photons is negligible small. This sets the initial condition, which resembles the Freeze-In mechanism. The calculations of the Yield equation get complicated so we will leave them once again out of the main body of the thesis, and can be found in Appendix *D*.

After the calculations we find that the density parameter is related with the mixing angle $\chi_0$ and the mass of the Dark Photon $m_{\gamma\prime}$ directly:

$$\Omega_{\gamma\prime} h^2 = \chi_0^2 m_{\gamma\prime}^3 9.27 \times 10^{37} \text{ GeV}^{-3} . \tag{2.15}$$

This sets a linear direct correlation depending on how much part of all Dark Matter is accounted by the Dark Photon via kinetic mixing. We can adjust the mass of the Dark Photon and the mixing angle so we get the correct relic abundance of Dark Matter. For example, if we wanted Dark Photons to account for 100% or 10% or just 1% (black, blue and orange line respectively in *Figure 2.7*) of the Dark Matter on the Universe we would have to adjust $\Omega_{\gamma\prime} h^2$.

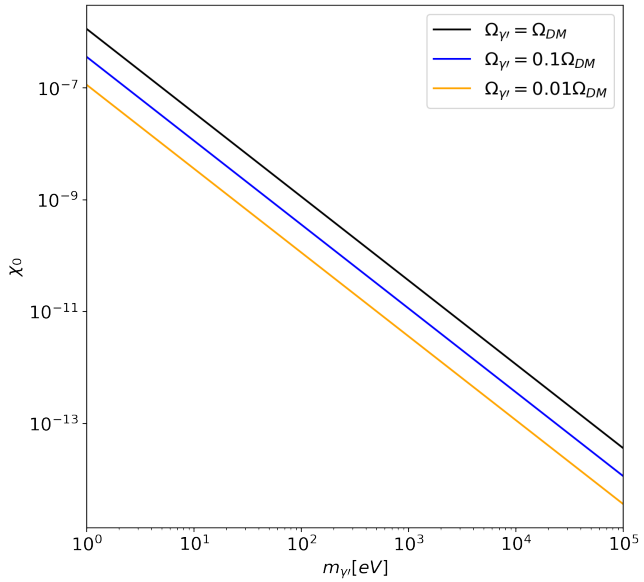


*Figure 2.7: Mass of the Dark Photon against the mixing parameter. The lines correspond to* 100%, 10% *and* 1% *(black, blue and orange respectively) of all Dark Matter in the Universe in the form of Dark Photons created through kinetic mixing.*

We can compare this results to the known constraints in the relation Dark Photon mass/mixing parameter (see [58]), as shown in *Figure 2.8*. It can be seen how there is little to no free parameter

space in the explored range (except a little near 0.1 MeV). This is due to the fact that with a very little initial Dark Photon number density, the required mixing is too big, and therefore excluded from modern experiments.

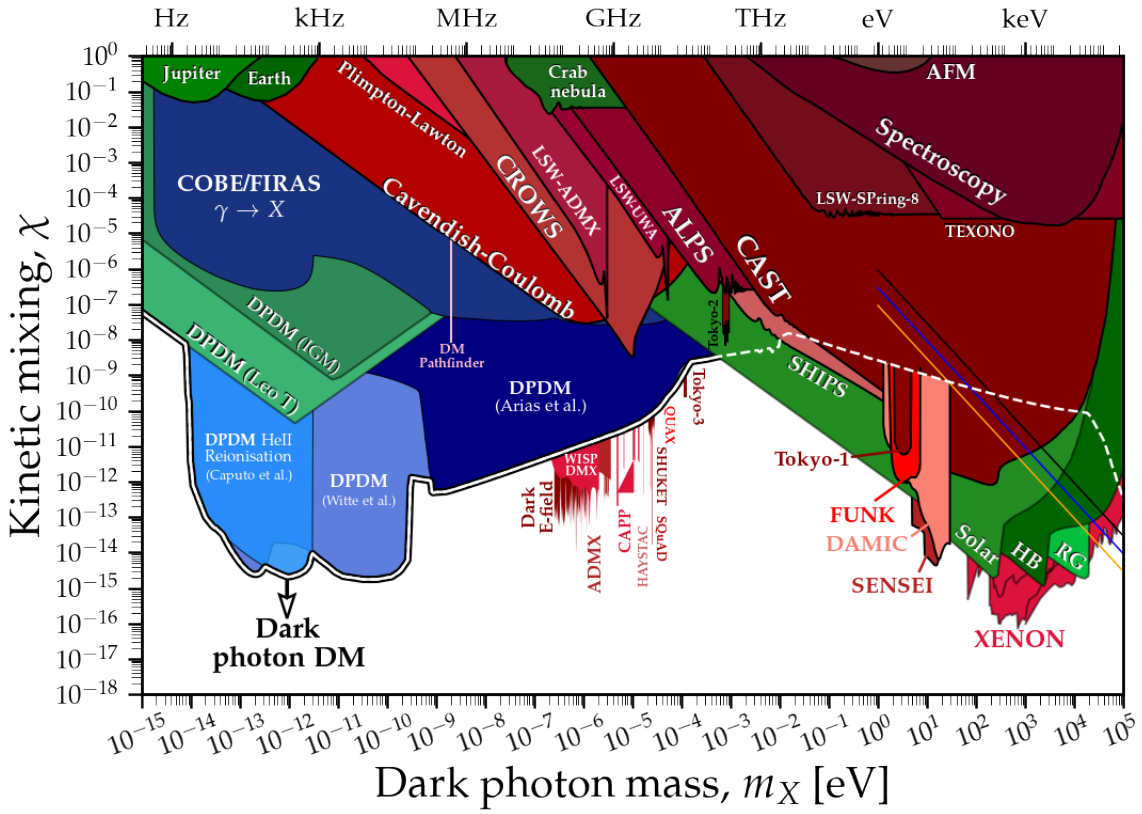


*Figure 2.8: Constraints on the kinetic mixing model taken from [58]. Some lines have been added in the range between* $1\text{eV} < m_{\gamma'} < 0.1\text{MeV}$ *corresponding to* 100%, 10% *and* 1% *(black, blue and orange respectively) of all Dark Matter in the Universe in the form of Dark Photons created through kinetic mixing.*

We could extend this model to Freeze-Out regions (with a non-zero initial number density of Dark Photons), or get to higher masses of the Dark Photons, but we will try to merge this model with the one from **Section 2.1** for low masses of the Dark Photon ($1\text{ eV} < m_{\gamma'} < 1\text{ MeV}$), in order to find a model that can account for all Dark Matter in the Universe, while being detectable by a direct search experiment such as DAMIC-M.

## 2.3 Dark Axion Portal

Now that we have checked and understood how the Dark Photon mixes with the photon and how the Dark Axion Portal works in general terms we can try to fix both models by putting them together. Axions producing Dark Photons was an undetectable model, but if Dark Photons are kinetically mixed with Standard Model photons, then they can interact electromagnetically and scatter of electrons and even be absorbed by electrons. This can improve the detection prospects drastically. But first, we will check the new constraints that arise from including the kinetic mixing ($\chi \neq 0$) in the Dark Axion Portal.

If the kinetic mixing is allowed, then the Dark Photon is allowed to decay to three photons so that the decay width is [72]:

$$\Gamma(\gamma\prime \to 3\gamma) \approx \left(5 \times 10^{-8}\right) \chi^2 \left(\frac{e^2}{4\pi^2}\right)^4 \left(\frac{m_{\gamma\prime}^9}{m_e^8}\right) . \tag{2.16}$$

This decay width imposes a constraint on the maximum mass of the Dark Photon, so the decay time is larger than the age of the Universe ($(13.79 \pm 0.02) \times 10^9$) years, if it was smaller all the Dark Matter would be photons by now and we would have noticed and wouldn't be able to detect any Dark Photon). The constraint becomes $m_{\gamma\prime} < \left(\frac{3.4175\times10^{26}}{\chi^2}\right)^{\frac{1}{9}}$. The smaller the value of $\chi$, the larger the maximum value for the mass of the Dark Photon, and for a value already constrained at low masses by Sensei, $\chi = 10^{-14}$, the constraint is $m_{\gamma\prime} < 1.15$ MeV, already out of our window (as we are not searching for Dark Photons heavier than 0.1 MeV). Thus, we don't have to worry about this decay mode.

The Dark Axion Portal opens other decay modes. One is a Dark Photon decaying to a electron-positron pair, but this decay is kinematically forbidden at the energy scale we are considering, so it is not worrying. The other one is a Dark Photon decaying to an axion and a photon:

$$\Gamma(\gamma\prime \to \gamma a) = \frac{G_{a\gamma\gamma\prime}^2}{96\pi} m_{\gamma\prime}^3 \left[1 - \frac{m_a^2}{m_{\gamma\prime}^2}\right]^3 . \tag{2.17}$$

As shown in eq. (2.4), this coupling is greatly suppressed by $\chi$, so the constraint on $m_{\gamma\prime}$ is always wider than the Dark Photon to three photons decay.

Axions are also subject to decay. The decay modes of the axion are to two photons, two Dark Photons, or a photon and a Dark Photon. However, the constraints that these decays impose on $f_a$ or on $m_{\gamma\prime}$ are less demanding than the available window of $f_a$ or the ones already imposed on $m_{\gamma\prime}$ from the Dark Photon decay.

At this point we can work freely, not having to worry about Dark Photons or axions disappearing from our Universe. We now know that for a non-excluded value of the kinetic mixing parameter the production of Dark Photons is negligible: if we take a kinetic mixing of $\chi = 3 \times 10^{-15}$, which is just a little above Sensei detection limits, then the density parameter coming from kinetic mixing

at $m_{\gamma\prime} = 20$ eV is $\Omega_{\gamma\prime}h^2 \sim 10^{-13}$. Therefore when merging both models, Dark Photon production via kinetic mixing is negligible, so all Dark Photons come from the gluon-gluon annihilation process (Freeze-In or Freeze-Out mechanism).

Then the production mechanism is the same as in the first model explained in **Section 2.1**, but the detection should be enhanced at low Dark Photon masses. This is because Dark Photons can now be scattered and (especially important for DAMIC-M) absorbed by electrons, because of their kinetic mixing. Now that we have a final theoretical model knowing its implications for cosmology, its detectability will be proved in **Chapter** *3*, but before that, we will make an important note on Cold and Warm Dark Matter, and the thermalization of these axions and Dark Photons in this model.

## 2.4 Note on Cold Dark Matter

We haven't talked much about the thermalization processes of Dark Photons and axions. Cold (or Warm [73] [74]) Dark Matter is needed in the Early Universe to explain large scale structure and the features in the Cosmic Microwave Background power spectrum. Hot Dark Matter, i.e. high energy relativistic particles, break structure with their high speed motions, and galaxies and clusters are unable to form. Therefore, we need to take a look at how relativistic will the particles in this model be, to see if they can account for Cold or at least Warm Dark Matter.

It is easy for axions, as they are produced by a non-thermal mechanism, the misalignment mechanism. Therefore, axions act as Cold Dark Matter right away, since they were born.

On the other hand, Dark Photons can be produced by Freeze-Out or Freeze-In. By Freeze-Out we have to clear regimes showed in *Figure 2.5*: a relativistic Freeze-Out in which Dark Photons would act as Hot Dark Matter, and a non-relativistic Freeze-Out, which would make them act as Cold Dark Matter, but is in the WIMP regime, in which we are not much interested at this point. By Freeze-In, the Dark Photons will inherit the temperature of the particles that create them, as they do not enter thermal equilibrium. But as Freeze-In happens very early in the Universe, the high energy of the gluons that annihilate would still make them somewhat relativistic.

Thankfully we have both species to work with, so it doesn't really matter if there is some Hot Dark Matter, as long as there is sufficient Cold Dark Matter to take care of the large scale structure, etc. Even more, having some Hot Dark Matter along with Cold Dark Matter, could solve the actual issues with Cold Dark Matter alone. This issue is addressed in [75], where they conclude with *Figure 2.9* the allowed density fraction of a Non-Cold Dark Matter particle, depending on its mass.

It can be seen how for large masses (near to the MeV) any particle would become non-relativistic soon enough in the history of the Universe, becoming Cold Dark Matter, so the fraction of early Cold Dark Matter needed is almost 0. However, for the mass range we are looking for, especially for Dark Photon absorption (1-100 eV), the fraction of Hot Dark Matter allowed (in our case Dark Photons) would be between 1% and 10% of the whole Dark Matter. Therefore, if we want to go

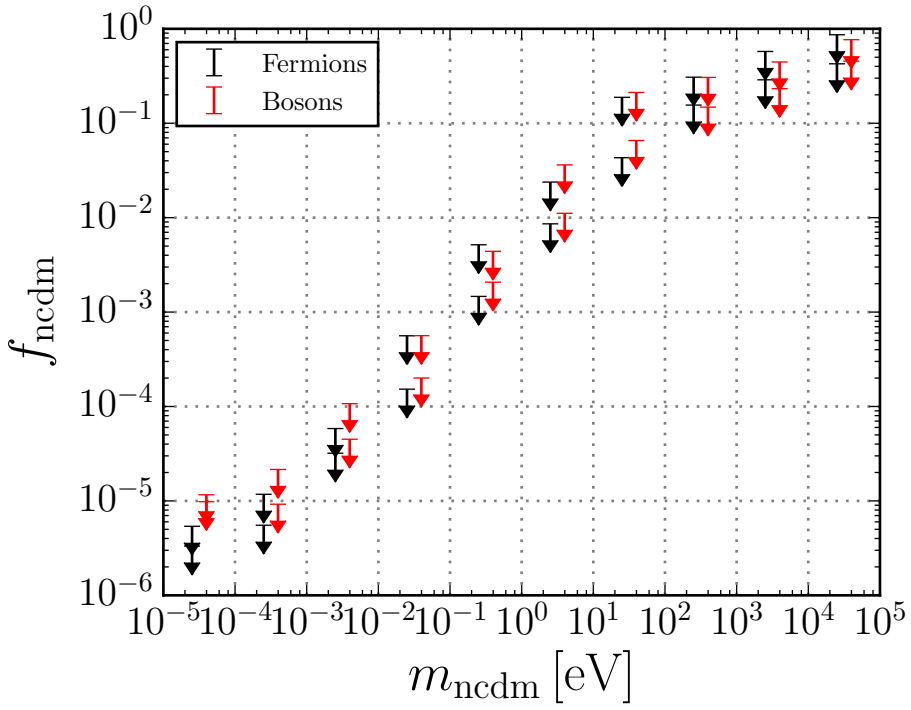


*Figure 2.9: Maximum fraction density of a Non-Cold Dark Matter particle needed to take account of the problems which Cold Dark Matter solves (large scale structure, CMB, BAO, etc.) as a function of the mass of this Non-Cold Dark Matter candidate. Figure taken from [75].*

to lower masses, we have to make axions be a larger fraction of all Dark Matter, and leave Dark Photons as a little fraction, say 1%. Thankfully, this was already needed if we wanted to take Dark Photons to lower masses, due to the Freeze-In constraint in the mass of the Dark Photon (check *Figure 2.4*). That way, leaving Dark Photons to 1% of the total Dark Matter density in the Universe allows us to account for all the needed Cold Dark Matter in the Universe as axions, while letting us reach 1.6 eV mass of the Dark Photon even by Freeze-In (see *Figure 2.10*).

All in all, this settles the idea of Dark Photons being just a little (1%) fraction of all Dark Matter, leaving the rest as either only axions (as the other 99%), or axions plus a whole hidden sector filled with Cold Dark Matter.

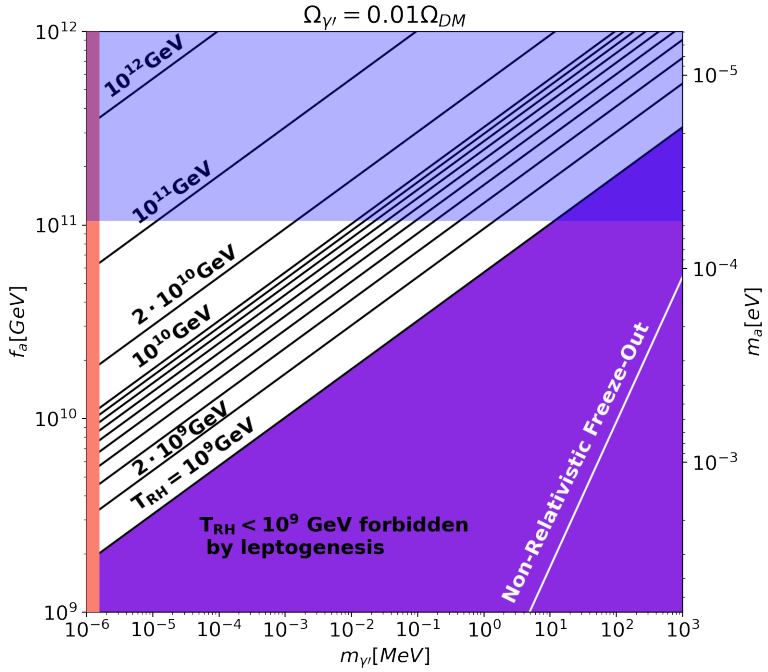


*Figure 2.10: Figure 2.5 with* $\Omega_{\gamma'}h^2 = 0.0012$, $\Omega_a h^2 = 0.1188$ *assuming all DM is axions (99%) + Dark Photons (1%).*

# 3 | Detectability

In this chapter we will explore the detectability of the model explained in **Chapter** *2*, first looking at the background noise in the LBC and then checking the Dark Photon absorption rate for the model.

Simulations have been done in order to probe the detectability of the Dark Photons in the DAMIC-M's proof of concept, the LBC. Impurity-induced background in the LBC is simulated using Monte Carlo methods by putting a lot of radioisotopes ($5 \times 10^7$) in each part of the LBC geometry (see *Figure 3.1*) and mimicking the CCD response to the particles that get to it. Then we get a whole energy density spectrum, which we normalize to the known values of the radioactivity of the materials used to build the final Low Background Chamber.

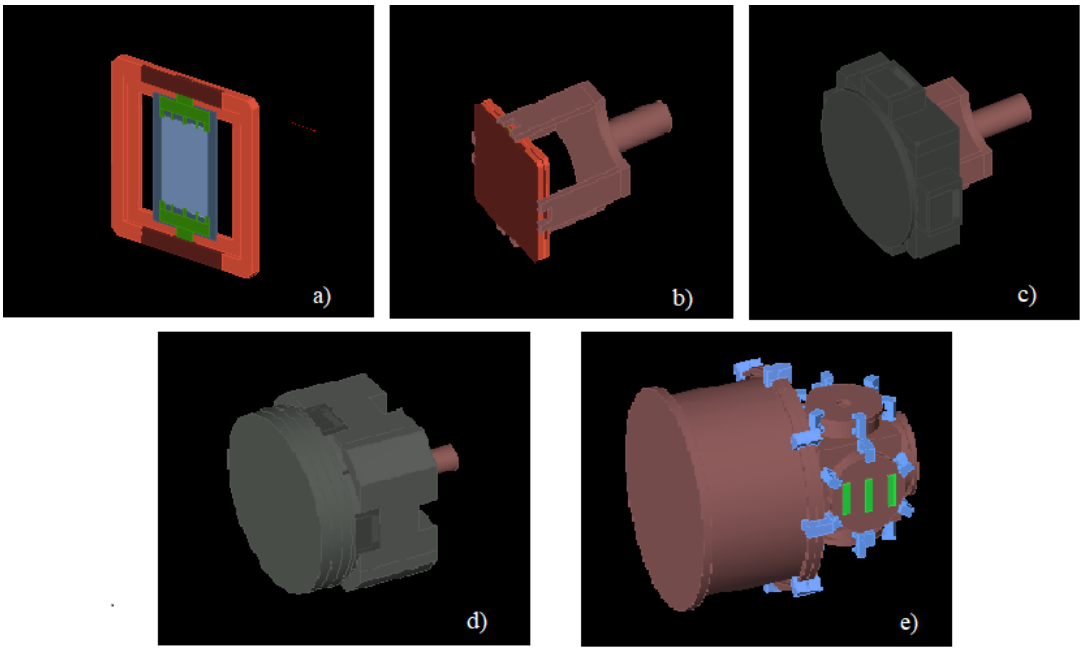


*Figure 3.1: a) CCD module including the sensitive detector zone (light blue), kapton cable (green) and copper frame (orange). b) Copper box holding both CCD modules. c) Roman lead layer. d) "New" lead layer covering the Roman one. e) Whole LBC geometry including cryostat layer. In light blue are represented holder pieces and in green the electronic input for the cryostat.*

The LBC geometry consists in:

- A sensitive detector: two 4000x6000 pixels (15x22.5 $\mu m$, 675 $\mu m$ thick) CCDs composed of

silicon and polysilicon layers.

- Kapton cables, for the electronic imput.
- A copper frame for the CCDs.
- Roman lead (taken from a spanish galleon) for protecting the CCDs from ionizing radiation while not radiating itself (because of being old, the decay time for lead nuclear chain has already passed and thus it does not induce more background noise).
- "New" lead extra layer (new lead is cheaper and easier to find than the old one and radiopurity this far from the sensitive detector is unnecessary).
- External cryostat to maintain the temperature at around 130 K.

The final experiment also has a 30 cm polyethylene external layer in order to provide a shielding against high energy gammas, neutrons from cosmic rays and nuclear decays, preventing nuclear activation. The shielding works due to the high content of hydrogen atoms in polyethylene. It is not necessary for the purposes of this simulation, as its possible background noise hardly reaches the CCD, making it totally negligible.

The software used to mimic the response of the DAMIC-M CCDs is composed of two packages: **DAMICG4** and **psimulCCDimg**

- **DAMICG4** performs Geant4-based simulations of the detector; being Geant4 a C++ framework which relies on Monte Carlo (MC) modelling to emulate physical processes [76];
- **psimulCCDimg** is a Python3 module used to reconstruct the response of the detector [77].

A more extensive explanation on how Geant4 and psimulCCDimg work can be found in [78], here we will try to summarize each software's functionality within this thesis.

DAMICG4 is a Monte Carlo simulation software that, roughly speaking, simulates the passing of particles through the detector by simulating its fundamental interactions with the different materials, guided by a list of physical processes that are given probability values. The processes a particle undergoes are chosen according to said probabilities at every "step" (a short distance within the materials at which the software evaluates the properties of the particle and where it is). This simulated particles could create secondaries due to its interaction, which are also tracked. The output of the simulation is a collection of geometrical points inside the detector (in our case the CCDs) where the particles have lost energy.

The energy loses inside the CCDs feed psimulCCDimg, a Python3 module that mimics the CCD response converting the energy losses in electron-hole pairs, drifting and diffusing the charges as if they were collected in a real CCD, pixelizing the signal and simulating the detector noise (dark current and readout noise, as mentioned in **Section 1.3.1**).

In our case, we are interested in simulating the radio-impurities in the LBC materials and the background noise they generate. For this purpose we start generating radioactive nuclei with no initial kinetic energy in each volume of the LBC geometry (check **Section 1.3.1**), so they start static in the geometry and then decay creating the decay products (electrons, positrons, alphas, neutrinos...) that move, interact and end reaching the CCDs.

The simulated isotopes belong to several decay chains ($^{238}$U, $^{226}$Ra, $^{210}$Pb and $^{232}$Th), but are simulated individually and decay one by one instead of simulating the whole chain. In *Table 3.1* you can find all the radioactive isotopes simulated.

| Parent Chain | Isotopes Considered | Comments |
|---|---|---|
| $^{238}$U | $^{234m}$Pa<br>$^{234}$Th | |
| $^{226}$Ra | $^{214}$Pb<br>$^{214}$Bi | |
| $^{210}$Pb | $^{210}$Pb<br>$^{210}$Bi | |
| $^{232}$Th | $^{228}$Ac<br>$^{228}$Ra<br>$^{212}$Pb<br>$^{212}$Bi<br>$^{208}$Tl | |
| $^{40}$K | $^{40}$K | |
| Activation | $^{56}$Co<br>$^{57}$Co<br>$^{58}$Co<br>$^{60}$Co<br>$^{59}$Fe<br>$^{54}$Mn<br>$^{46}$Sc | Only in Copper parts, and if it is not electroformed copper. All of them produced in the copper by spallation. |

*Table 3.1: Decay chains considered in this analysis.*

To find the energy spectrum these isotopes leave, we simulate $5 \times 10^7$ of each one in each volume, distributed uniformly, so we have a large enough statistic. Then, in order to find the correct induced spectral background, we need to normalize said large statistic to the real number of events we would find in the experiment. The normalization is done with the following equation:

$$n^{\text{norm}}_{\text{clusters}}(E_i) = n^{\text{sims}}_{\text{clusters}}(E_i) \frac{1}{N_{\text{sims}}} A_{\text{isotope}} M_{\text{simvol}} \frac{1}{M_{\text{detector}}} \frac{N_{\text{bins}}}{E_{\text{max}} - E_{\text{min}}}\,, \tag{3.1}$$

where:

- $n^{sims}_{clusters}(E_i)$ is the total number of clusters (individual energy deposits in the CCD) in the energy bin centered at $E_i$.
- $N_{sims}$ is the total number of simulations ($5 \times 10^7$ in this case).
- $A_{isotope}$ is the activity of the isotope at the simulated volume, in units of decays/day/kg of the material forming the simulated volume.
- $M_{simvol}$ is the total mass of the simulated volume, in units of kg.
- $M_{detector}$ is the total mass of the simulated detector, in units of kg.
- $E_{max} - E_{min}$ is the full energy range evaluated in the spectrum, in keV.
- $N_{bins}$ is the total number of energy bins in the range $[E_{max}, E_{min}]$, uniformly distributed.

This normalization allows us to find the correct background noise generated by each isotope in each volume, in units of decays/kg/day/keV (the keV part is to eliminate the effects of the binning in the simulated spectrum and kg refer to the detector's mass).

In order to determine the induced spectral background, we need the activity of each isotope in each component of the detector ($A_{isotope}$ in eq. (3.1)). For LBC simulation studies we will use the contamination levels obtained on the DAMIC analysis. Said levels can be found in *Table 3.2*.

| Part | U-238 | Ra-226 | Pb-210 | Th-232 | K-40 |
|---|---|---|---|---|---|
| CCD | <0.53 | <0.43 | <33 | <0.4 | <0.04 |
| Kapton cable | 5013.8 ± 423.4 | 420 ± 490 | 420 ± 490 | 276.5 ± 42.0 | 2475.4 ± 172.8 |
| Copper | <10.7 | <10.7 | 2350 ± 720 | <3.5 | <2.7 |
| Module Screws | 1400 ± 3800 | <138 | 2350 ± 720 | 200 ± 140 | 2400 ± 1300 |
| Ancient lead shield | <10.7 | <25.9 | 2850 ± 285 | <2.8 | <0.5 |
| Outer lead shield | <1.1 | <13 | 1560000 ± 430000 | <0.4 | <19 |

*Table 3.2: DAMIC activities used to constrain the amount of radioactivity in each component in units of decays/kg/day. In the case of the Copper, the measurements come from various sources (DAMIC100, Canfranc) as the new electroformed copper will be used.*

Now that it has been explained how the background simulations are done and normalized, it can be better understood with an example. We will use the Kapton cable, as all of the isotopes mentioned in *Table 3.1* are important in this volume. First all isotopes are simulated individually, with $5 \times 10^7$ isotopes equally distributed through the whole volume. Then the energy deposits of each one is plotted, see for example the one for $^{234m}$Pa in *Figure 3.2*.

Once we know the energy deposit we can normalize the histogram according to eq. (3.1), in this example with $^{234m}$Pa, known that the Kapton cable mass is 5.81 grams, the mass of one CCD is 8.49 g, and using 100 bins between 0 and 20 keV. We scale *Figure 3.2* resulting in *Figure 3.3*.

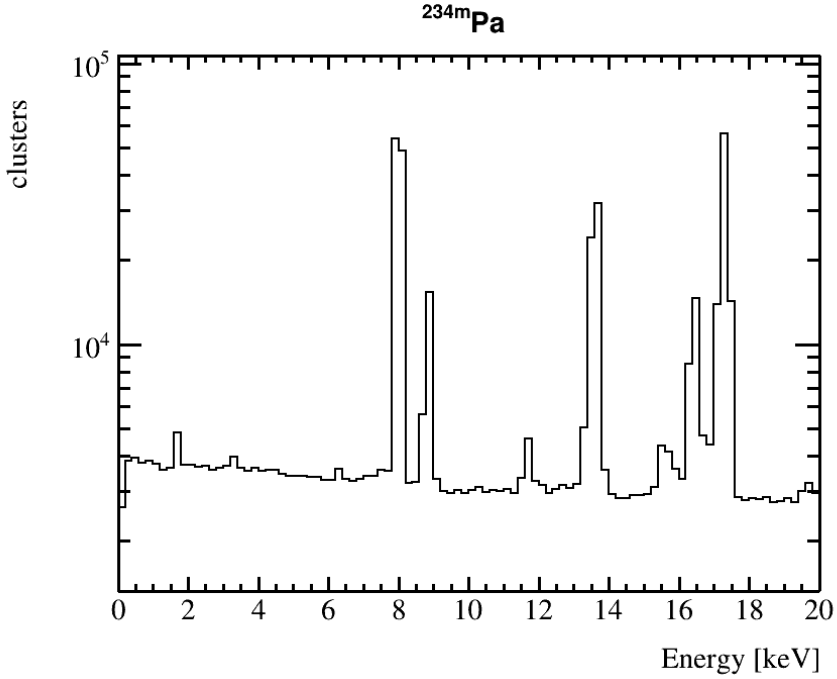


*Figure 3.2: Simulated background noise induced by $5 \times 10^7$ isotopes of $^{234m}Pa$ in the Kapton cable of the LBC.*

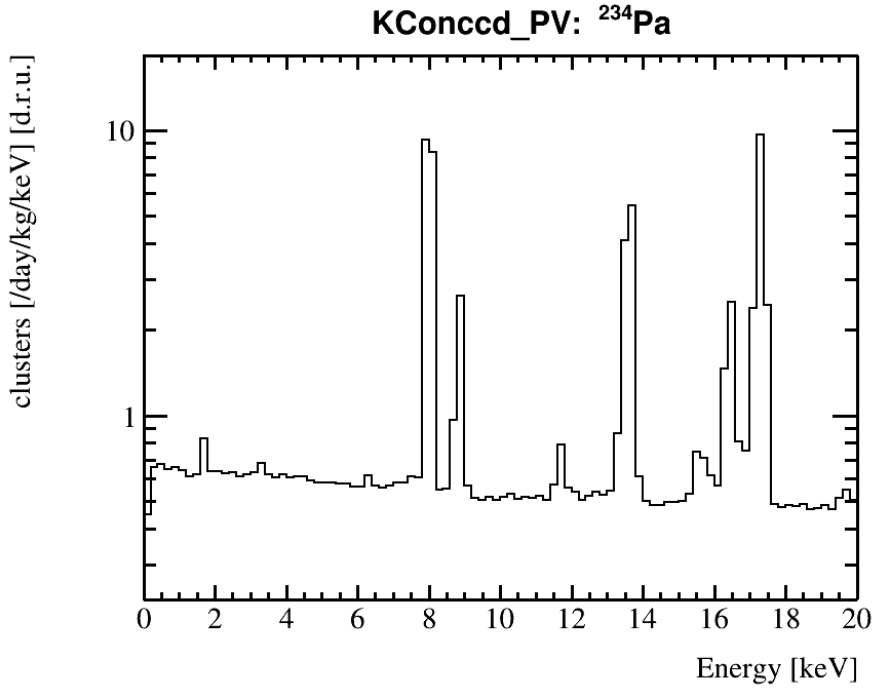


*Figure 3.3: Simulated background noise induced by $^{234m}Pa$ in the Kapton cable of the LBC as in Figure 3.2, but rescaled for the values expected in the LBC, in units of decays/kg/day/keV.*

At this point to know the background noise, we want the peaks to be excluded (as they can be subtracted knowing the radioisotopes typical emission lines), so the wanted data is the detection limit imposed by the Compton background (the flat noise). In order to do this, we fit the histogram to a constant as $y = a$ in a zone with no emission peaks, in this case between 2 and 6 keV, finding for this particular case that the $^{234m}$Pa from the Kapton cable induces 0.605±0.002 decays/kg/day/keV.

Extrapolating this example to every isotope we can sum them all up to know the whole noise induced by the Kapton cable volume, which is shown in *Figure 3.4*.

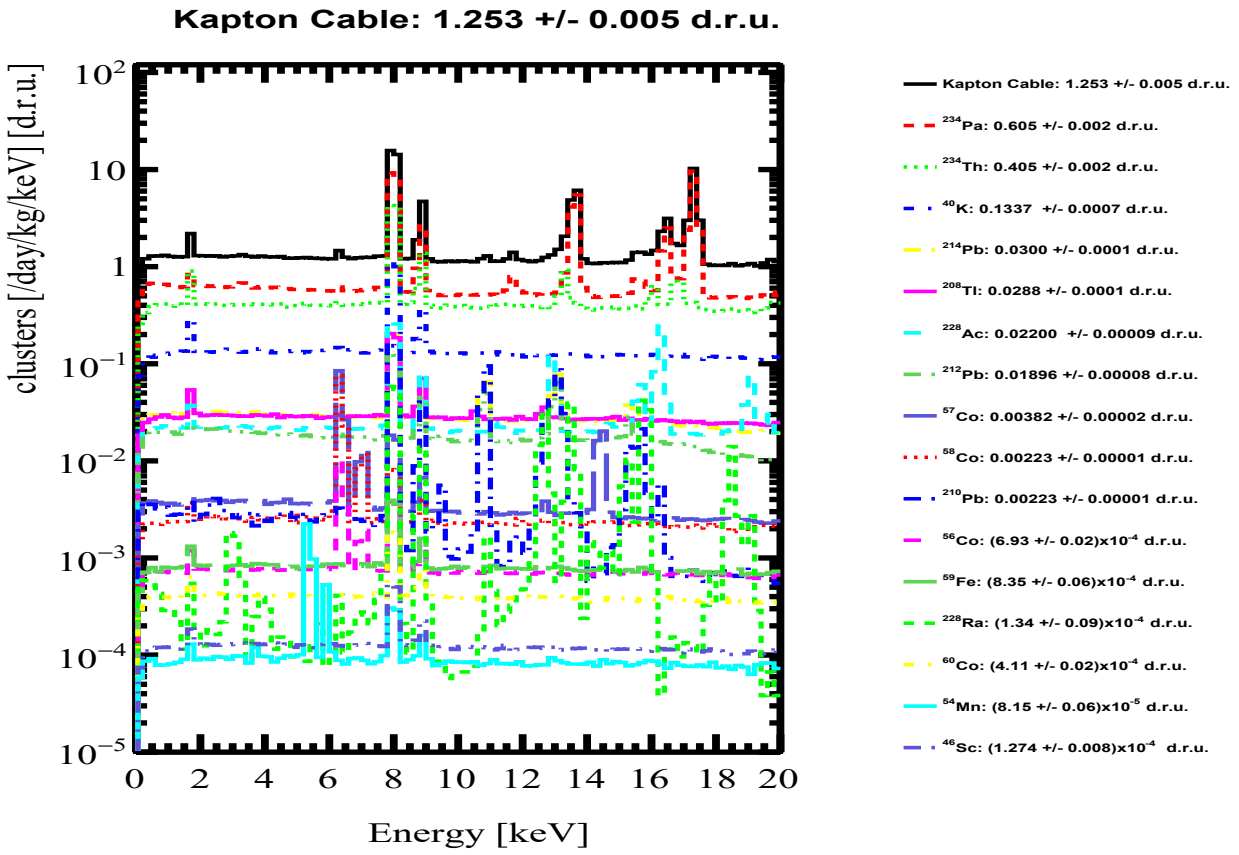


*Figure 3.4: Background noise induced by every isotope and the total of the Kapton cable of the LBC in units of clusters/kg/day/keV.*

It couldn't be unnoticed by a watchful eye how *Figure 3.4* is missing all Bismuth isotopes included in *Table 3.1*. This was caused by a bug on the new version 10.06 of DAMICG4 and is intended to be corrected soon.

Extending the work done with the Kapton Cable to all the volumes in the LBC geometry (Copper frame holding the CCDs named ColdCopper, Roman Lead called AncientLead and "'New Lead" called LBLead), we can obtain the complete background noise in the LBC. This is shown in

*Figure 3.5.*

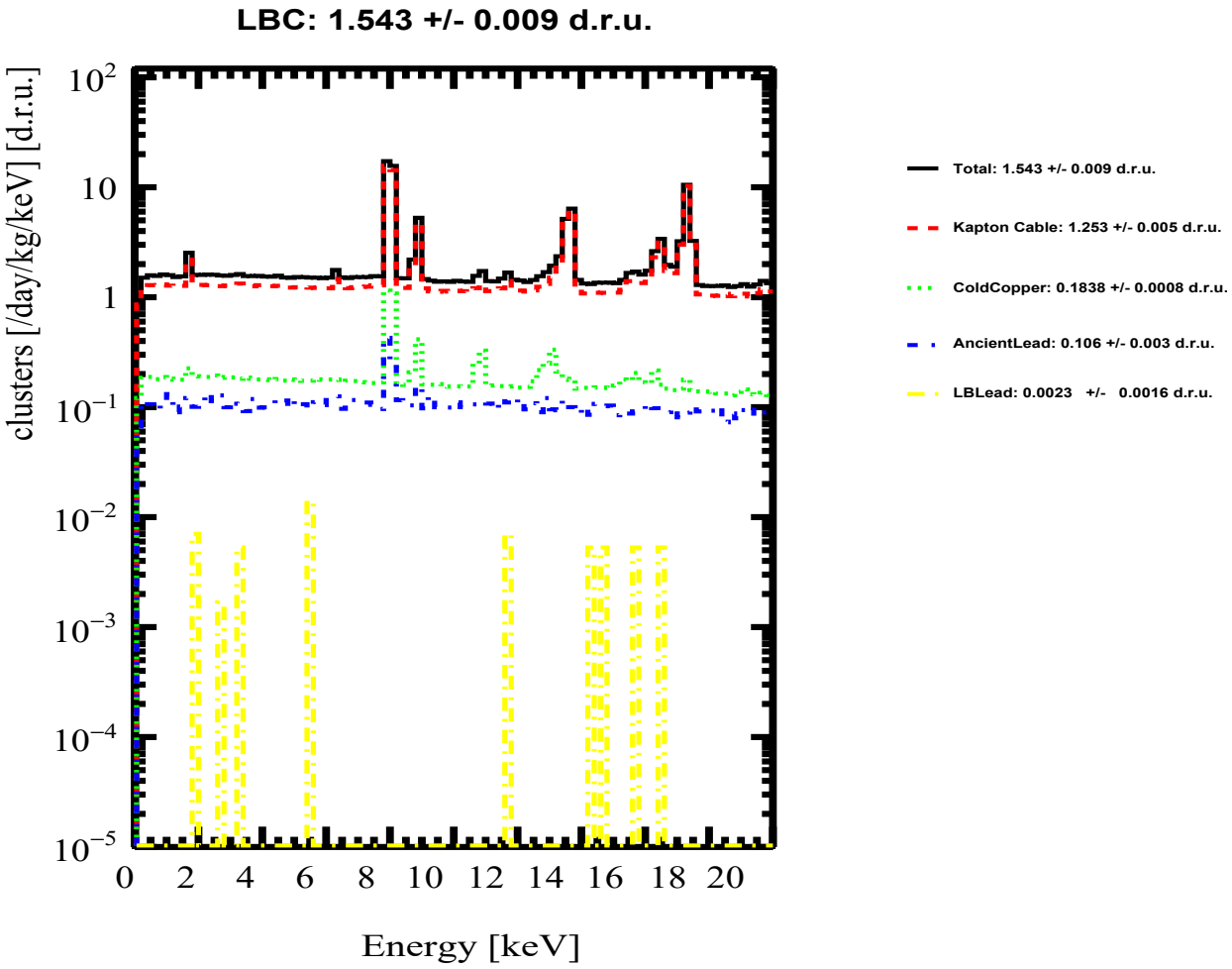


*Figure 3.5: Background noise induced by every volume and the total of the LBC in units of decays/kg/day/keV.*

Like this we have obtained the background noise induced by isotopes in the LBC. Because of the bug in Bismuth, and although at low energies (below 0.1 keV) the background noise is reduced (there is less low energy ionization), we will keep a conservative approach by taking the background noise as 3 clusters/day/kg/keV.

It is important also to remember the other noise sources, which include the readout noise and the dark current. As explained in **Section 1.3.1** the readout noise is negligible. With DAMIC having the lowest dark current ever measured in a silicon detector, the dark current only constrains the measurement below two electrons (7.54 eV).

## 3.1 Dark Photon absorption rate

Now that we know the expected background noise in the LBC, it has to be compared with the Dark Photons signal, especially looking at the Dark Photon absorption rate. Dark Photon absorption signal should be seen as a peak of electrons with an energy $E \sim m_{\gamma\prime}$.

The absorption cross-section of a Dark Photon $\sigma_{\gamma\prime}(m_{\gamma\prime})$ with velocity $v$ is directly related with the photoelectric cross section for a photon with energy $m_{\gamma\prime}c^2$, $\sigma_\gamma(m_{\gamma\prime}c^2)$ [55, 79, 80, 81] as:

$$\sigma_{\gamma\prime}(m_{\gamma\prime})v = \chi^2\sigma_\gamma(m_{\gamma\prime}c^2)c\,. \tag{3.2}$$

This allows us to account for the rate of absorbed Dark Photons in a target as:

$$R = \frac{\rho_{DM}}{m_{\gamma\prime}}\chi^2\sigma_\gamma(m_{\gamma\prime}c^2)c\,, \tag{3.3}$$

where $\rho_{DM}$ is the local density of Dark Matter composed by Dark Photons ($\rho_{DM} = 0.3$ GeV $c^{-2}$ cm$^{-3}$ if Dark Photons accounted for 100% of Dark Matter).

Now we can get the values of the photoelectric cross section in silicon (Above 10 eV: [82] and below 10 eV: [83] [84]) and check the rate of absorbed Dark Photons (assuming they account for 100% of the Dark Matter of the Universe) per kg of detector and per day, as shown in *Figure 3.6*.

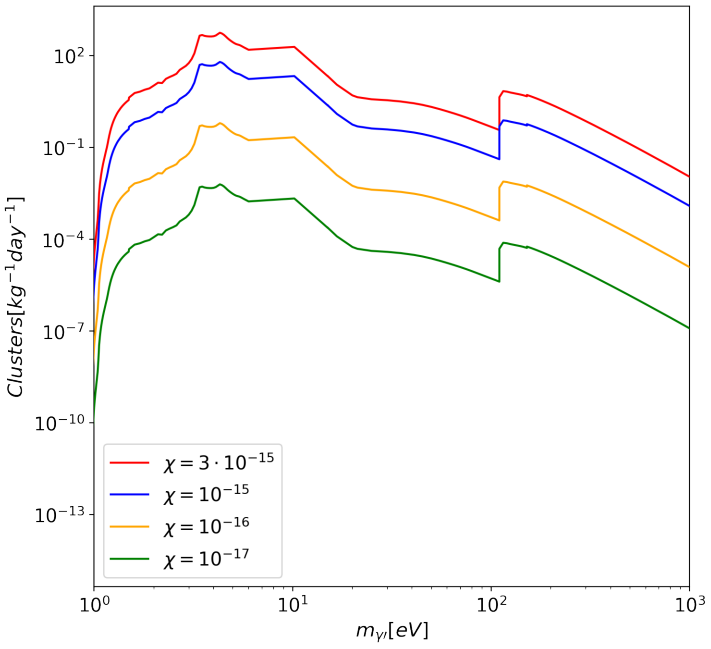


*Figure 3.6: Absorption rate of Dark Photons ($\Omega_{\gamma\prime}h^2 = 0.12$) in silicon as a function of $m_{\gamma\prime}$.*

At this point, we have a rough estimate of the detector sensitivity. We can determine the rate of Dark Photons absorbed in a detector for the Dark Axion Portal model (i.e. Dark Photons being 1% of the total Dark Matter), and compare it to the background noise to check if the absorption of Dark Photons will leave a peak in the detected spectra. This is shown in *Figure 3.7*.

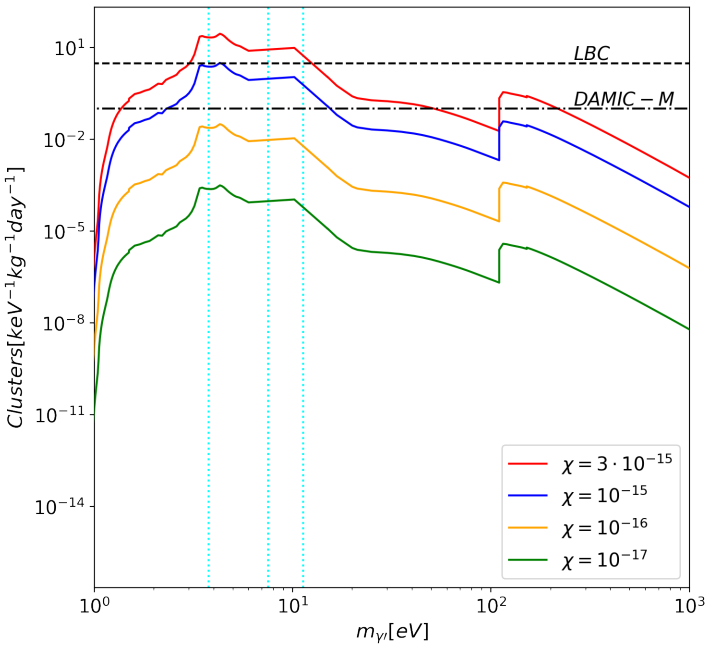


*Figure 3.7: Absorption of Dark Photons ($\Omega_{\gamma\prime} = 0.01\Omega_{DM}$) in silicon, compared with the background noise of the LBC $\approx 3\ kg^{-1}day^{-1}keV^{-1}$, and the expected from DAMIC-M $\approx 0.1\ kg^{-1}day^{-1}keV^{-1}$. The cyan vertical dotted lines represent 1, 2 and 3 electrons (3.77, 7.54 and 11.31 eV respectively), as because of the dark current, we can detect 3 electrons or more.*

It can be seen how the model can be detected even in the LBC (which was not first intended for detection but for R&D), as the signal is over the noise at an energy of 3 electrons (which is no longer obscured by dark current). This shows the detection power of the DAMIC-M experiment and especially the new skipper CCDs.

# 4 | Conclusions

In this thesis we have studied direct Dark Matter searches end to end, from exploring a theoretical model for particle Dark Matter and its implications for cosmology, with Dark Photons and axions as the candidates, to examining the detectability of said Dark Photons in a particular direct search experiment, DAMIC-M (in particular, its proof-of-concept, the LBC).

For the theoretical model, the Dark Axion Portal has been studied, exploring a connection between axions and Dark Photons. Pairs of Dark Photons are created via annihilation of gluons, mediated by the axion in the Early Universe. This happens through the Freeze-In mechanism, which opens a wider parameter space for the properties of both the axion and the Dark Photon than the Freeze-Out mechanism. Another connection of this portal to the Standard Model is the kinetic mixing of Dark Photons to Standard Model photons, which would create a negligible number density of Dark Photons, but would enhance the possibilities of direct detection.

Thanks to the possibilities provided by the Dark Axion Portal, the model can account for all Dark Matter in the Universe, while being Cold Dark Matter, with 1% Dark Photons and 99% axions. This is a promising scenario involving multi-component Dark Matter, which has prospects of detectability in the near future, as many experiments work on the detection of Dark Photons, and many on axions.

In order to illustrate the detectability of Dark Photons in a direct search experiment, simulations were done using the proof of concept of DAMIC-M, the LBC. The background noise induced by radioimpurities (from materials surrounding the detector) was simulated, while emulating the intrinsic detector noise at the same time. This allows us to know if we can discriminate the expected signal from Dark Photon absorption in the detector (see *Figure 3.6*) from the backgound noise in the LBC (see *Figure 3.5*). The result shows a possible detectability at low energies, which is very promising for the LBC, and is shown in *Figure 3.7*.

Said detectability allows us to include the LBC and DAMIC-M in the constraints on the kinetic mixing done in [58] (see *Figure 2.8*), by tuning the mixing parameter until the background rate and the signal rate match. It can be noted how these curves match the ones obtained in *Figure 3.7* but upside down because the kinetic mixing parameter is proportional to the rate of absorbed Dark Photons as stated in eq. (3.3). The constraints become even stronger if Dark Photons are set as all the Dark Matter in the Universe, instead of just a 1%. This is shown in *Figure 4.1*.

In conclusion, we have managed to find a model which can account for all Dark Matter in the Universe in the form of Dark Photons and axions, connected not only by their individual, already studied connections to the Standard Model, but by genuinely new couplings through the Dark Axion Portal. While accounting for just 1% all Dark Matter, the Dark Photons could be potentially

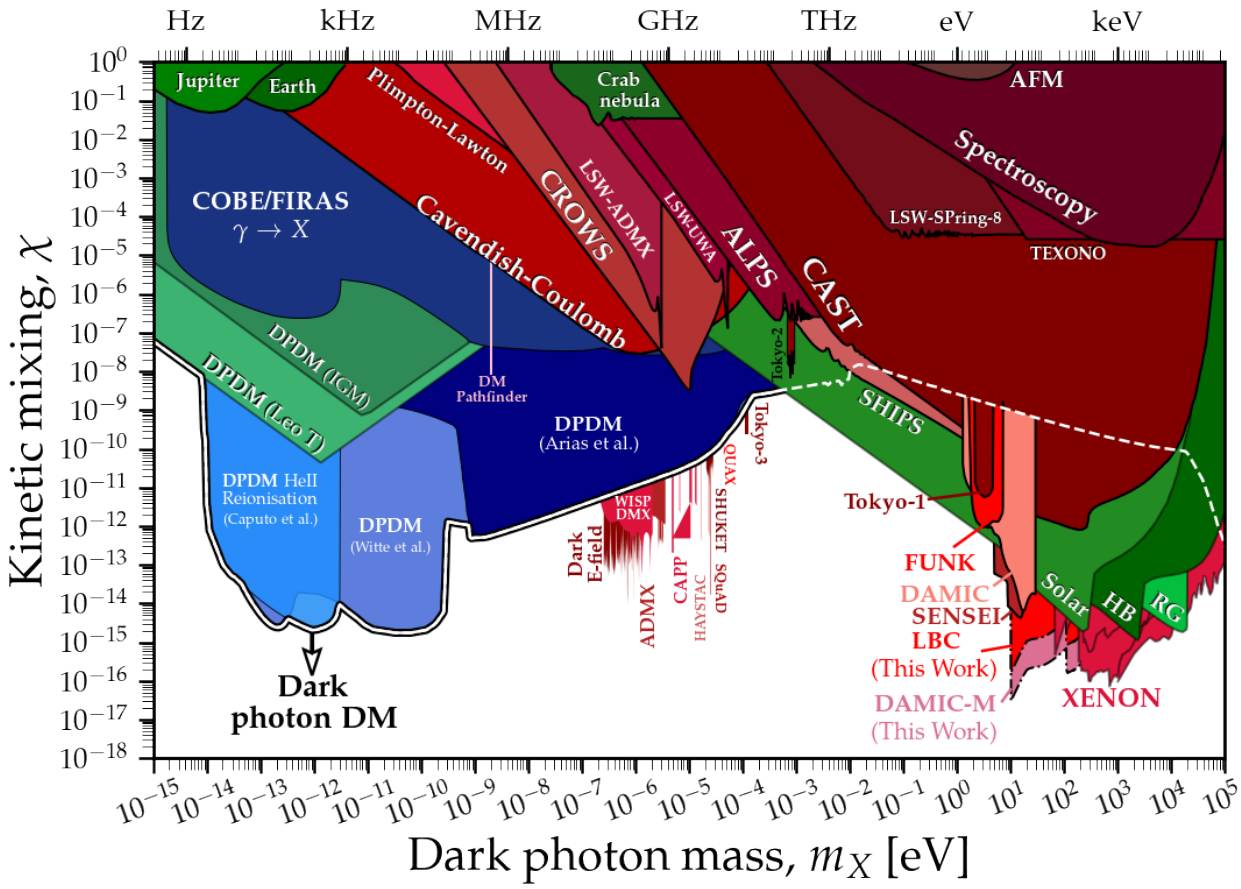


*Figure 4.1: Figure modified from [58] to include the constraints on the kinetic mixing parameter that will be imposed by the LBC and DAMIC-M.*

detected soon in the proof of concept of DAMIC-M, the LBC, and of course, DAMIC-M itself.

## 4.1 Future work

Dark Photons have been proven to have promising detectability prospects in new Dark Matter direct search experiments in what refers to Dark Photon absorption, however, the detection can be explored using electron scattering, or more detailed calculations on nuclear recoils, allowing us to open even more the range of masses for which Dark Photons would be detectable, especially in other types of direct search experiments which don't use CCDs (as the latter are particularly good for Dark Photon absorption).

As a future work is also left the axion detectability, which was out of the scope of this work, and would be a nice addition with enough time and knowledge on the field.

The Dark Axion Portal is also open to a wider parameter space, as it can reach higher Dark Photon masses, or can be filled with a much rich and varied hidden sector tuning the density of axions. Even some other scenarios can be considered, such as an initial condensate on Dark Photons in the Early Universe, which would enhance the number density of Dark Photons and rearrange the parameter space.

Also, an obvious future work on the lines of this thesis is to prove its limits once the LBC and DAMIC-M become operative, checking the simulations were correct and the noises were well estimated, and if the expected signal from Dark Photons is found or not.

All in all, the Dark Axion Portal sets a rich and promising scenario for particle Dark Matter and can lead to new, joint studies of Dark Photons and axions together, which could be done in the near future.

# Bibliography

[1] R. Essig, J. A. Jaros, W. Wester, et al. Dark sectors and new, light, weakly-coupled particles, 2013.

[2] Kunio Kaneta, Hye-Sung Lee, and Seokhoon Yun. Portal connecting dark photons and axions. *Physical Review Letters*, 118(10), Mar 2017.

[3] `http://pla.esac.esa.int/pla/`. Release from 2018, last visited 15/03/2020.

[4] Heinz Andernach and Fritz Zwicky. English and Spanish Translation of Zwicky's (1933) The Redshift of Extragalactic Nebulae. *arXiv e-prints*, page arXiv:1711.01693, November 2017.

[5] Vera C. Rubin and Jr. Ford, W. Kent. Rotation of the Andromeda Nebula from a Spectroscopic Survey of Emission Regions. *Astrophysical Journal*, 159:379, February 1970.

[6] J. G. de Swart, G. Bertone, and J. van Dongen. How dark matter came to matter. *Nature Astronomy*, 1(3), Mar 2017.

[7] Sidney van den Bergh. The Stability of Clusters of Galaxies. *Zeitschrift für Astrophysik*, 55:21, January 1962.

[8] D. H. Rogstad and G. S. Shostak. Gross Properties of Five Scd Galaxies as Determined from 21-Centimeter Observations. *Astrophysical Journal*, 176:315, September 1972.

[9] Jeremy L. Tinker, Brant E. Robertson, Andrey V. Kravtsov, Anatoly Klypin, Michael S. Warren, Gustavo Yepes, and Stefan Gottlöber. The large-scale bias of dark matter halos: Numerical calibration and model tests. *The Astrophysical Journal*, 724(2):878–886, Nov 2010.

[10] E. Komatsu, J. Dunkley, M. R. Nolta, C. L. Bennett, et al. Five-Year Wilkinson Microwave Anisotropy Probe Observations: Cosmological Interpretation. *The Astrophysical Journal Supplement*, 180(2):330–376, February 2009.

[11] Anne M Green and Bradley J Kavanagh. Primordial black holes as a dark matter candidate. *Journal of Physics G: Nuclear and Particle Physics*, 48(4):043001, Feb 2021.

[12] Carl H. Gibson. Fluid mechanics explains cosmology, dark matter, dark energy, and life, 2012.

[13] Jacob D. Bekenstein. Alternatives to dark matter: Modified gravity as an alternative to dark matter, 2010.

[14] A. Boyarsky, M. Drewes, T. Lasserre, S. Mertens, and O. Ruchayskiy. Sterile neutrino dark matter. *Progress in Particle and Nuclear Physics*, 104:1–45, Jan 2019.

[15] Javier Redondo and Marieke Postma. Massive hidden photons as lukewarm dark matter. *Journal of Cosmology and Astroparticle Physics*, 2009(02):005–005, Feb 2009.

[16] Luca Di Luzio, Maurizio Giannotti, Enrico Nardi, and Luca Visinelli. The landscape of qcd axion models, 2020.

[17] Riccardo Catena and Laura Covi. Susy dark matter(s). *The European Physical Journal C*, 74(5), May 2014.

[18] Giorgio Arcadi, Maíra Dutra, Pradipta Ghosh, Manfred Lindner, Yann Mambrini, Mathias Pierre, Stefano Profumo, and Farinaldo S. Queiroz. The waning of the wimp? a review of models, searches, and constraints. *The European Physical Journal C*, 78(3), Mar 2018.

[19] Gianfranco Bertone and Tim M. P. Tait. A new era in the search for dark matter. *Nature*, 562(7725):51–56, Oct 2018.

[20] Marco Battaglieri, Alberto Belloni, Aaron Chou, Priscilla Cushman, et al. Us cosmic visions: New ideas in dark matter 2017: Community report, 2017.

[21] Mirjam Cvetič, James Halverson, and Hernan Piragua. Stringy hidden valleys. *Journal of High Energy Physics*, 2013(2), Feb 2013.

[22] Sebastian Baum, Katherine Freese, and Chris Kelso. Dark matter implications of dama/libra-phase2 results. *Physics Letters B*, 789:262 – 269, 2019.

[23] Giulia D'Imperio. Dark matter search with the sabre experiment, 2018.

[24] D.S. Akerib, S. Alsum, H.M. Araújo, X. Bai, A.J. Bailey, J. Balajthy, P. Beltrame, E.P. Bernard, A. Bernstein, T.P. Biesiadzinski, et al. Results from a search for dark matter in the complete lux exposure. *Physical Review Letters*, 118(2), Jan 2017.

[25] Xiangyi Cui, Abdusalam Abdukerim, Wei Chen, Xun Chen, et al. Dark matter results from 54-ton-day exposure of pandax-ii experiment. *Physical Review Letters*, 119(18), Oct 2017.

[26] E. Aprile, J. Aalbers, F. Agostini, M. Alfonsi, L. Althueser, F.D. Amaro, et al. Dark matter search results from a one ton-year exposure of xenon1t. *Physical Review Letters*, 121(11), Sep 2018.

[27] C. Amole, M. Ardid, I.J. Arnquist, D.M. Asner, D. Baxter, E. Behnke, M. Bressler, B. Broerman, G. Cao, C.J. Chen, et al. Dark matter search results from the complete exposure of the pico-60 c3f8 bubble chamber. *Physical Review D*, 100(2), Jul 2019.

[28] R. Agnese, A.J. Anderson, M. Asai, D. Balakishiyeva, R. Basu Thakur, D.A. Bauer, J. Beaty, J. Billard, A. Borgland, M.A. Bowles, et al. Search for low-mass weakly interacting massive particles with supercdms. *Physical Review Letters*, 112(24), Jun 2014.

[29] G. Angloher, A. Bento, C. Bucci, L. Canonica, X. Defay, A. Erb, F. von Feilitzsch, N. Ferreiro Iachellini, P. Gorla, A. Gütlein, et al. Results on light dark matter particles with a low-threshold cresst-ii detector. *The European Physical Journal C*, 76(1), Jan 2016.

[30] Bob Holdom. Two u(1)'s and $\epsilon$ charge shifts. *Physics Letters B*, 166(2):196–198, 1986.

[31] R.D. Peccei and Helen Quinn. Cp conservation in the presence of pseudoparticles. *Physical Review Letters - PHYS REV LETT*, 38:1440–1443, 06 1977.

[32] R. D. Peccei and Helen R. Quinn. Constraints imposed by CP conservation in the presence of pseudoparticles. *Phys. Rev. D*, 16:1791–1797, Sep 1977.

[33] Roberto D. Peccei. The strong cp problem and axions. *Axions*, page 3–17, 2008.

[34] David J.E. Marsh. Axion cosmology. *Physics Reports*, 643:1–79, Jul 2016.

[35] C. Abel, S. Afach, N.J. Ayres, C.A. Baker, G. Ban, G. Bison, et al. Measurement of the permanent electric dipole moment of the neutron. *Physical Review Letters*, 124(8), Feb 2020.

[36] D Baumann. *Lecture notes: Cosmology.* Amsterdam Cosmology Group, University of Amsterdam and Nikhef, Amsterdam, 2020. `http://cosmology.amsterdam/education/cosmology/`. Last visited: 12/04/2021.

[37] Lawrence J. Hall, Karsten Jedamzik, John March-Russell, and Stephen M. West. Freeze-in production of fimp dark matter. *Journal of High Energy Physics*, 2010(3), Mar 2010.

[38] Raymond T. Co, Lawrence J. Hall, and Keisuke Harigaya. Axion kinetic misalignment mechanism. *Physical Review Letters*, 124(25), Jun 2020.

[39] Olivier Wantz and E. P. S. Shellard. Axion cosmology revisited. *Physical Review D*, 82(12), Dec 2010.

[40] Anson Hook. Tasi lectures on the strong cp problem and axions, 2018.

[41] Alvaro Chavarria, Javier Tiffenberg, et al. Damic at snolab, 2014.

[42] J. Angle, E. Aprile, F. Arneodo, L. Baudis, A. Bernstein, A. Bolozdynya, P. Brusov, L. C. C. Coelho, C. E. Dahl, L. DeViveiros, et al. First results from the xenon10 dark matter experiment at the gran sasso national laboratory. *Physical Review Letters*, 100(2), Jan 2008.

[43] P. Agnes, I.F.M. Albuquerque, T. Alexander, A.K. Alton, G.R. Araujo, M. Ave, H.O. Back, B. Baldin, G. Batignani, K. Biery, et al. Darkside-50 532-day dark matter search with low-radioactivity argon. *Physical Review D*, 98(10), Nov 2018.

[44] T. Aralis, T. Aramaki, I.J. Arnquist, E. Azadbakht, W. Baker, S. Banik, D. Barker, C. Bathurst, D.A. Bauer, L.V.S. Bezerra, et al. Constraints on dark photons and axionlike particles from the supercdms soudan experiment. *Physical Review D*, 101(5), Mar 2020.

[45] J. Amare, S. Cebrian, D. Cintas, I. Coarasa, E. Garcia, et al. Annual modulation results from three years exposure of anais-112, 2021.

[46] M Boezio, M Pearce, et al. PAMELA and indirect dark matter searches. *New Journal of Physics*, 11(10):105023, oct 2009.

[47] R. Caputo, M. R. Buckley, P. Martin, E. Charles, A. M. Brooks, A. Drlica-Wagner, J. Gaskins, and M. Wood. Search for gamma-ray emission from dark matter annihilation in the small magellanic cloud with the fermi large area telescope. *Phys. Rev. D*, 93:062004, Mar 2016.

[48] S. J. Asztalos, G. Carosi, C. Hagmann, D. Kinion, K. van Bibber, M. Hotz, L. J Rosenberg, G. Rybka, J. Hoskins, J. Hwang, et al. Squid-based microwave cavity search for dark-matter axions. *Physical Review Letters*, 104(4), Jan 2010.

[49] E. Aprile and others (XENON Collaboration). Dark Matter Results from 225 Live Days of XENON100 Data. *Phys. Rev. Lett.*, 109(18):181301, November 2012.

[50] Daniel Abercrombie, Nural Akchurin, et al. Dark matter benchmark models for early lhc run-2 searches: Report of the atlas/cms dark matter forum. *Physics of the Dark Universe*, 27:100371, 2020.

[51] N. Castelló-Mor. Damic-m experiment: Thick, silicon ccds to search for light dark matter. *Nuclear Instruments and Methods in Physics Research Section A: Accelerators, Spectrometers, Detectors and Associated Equipment*, 958:162933, Apr 2020.

[52] Torsten Åkesson, Asher Berlin, Nikita Blinov, Owen Colegrove, Giulia Collura, Valentina Dutta, et al. Light dark matter experiment (ldmx), 2018.

[53] A. Drukier and L. Stodolsky. Principles and applications of a neutral-current detector for neutrino physics and astronomy. *Phys. Rev. D*, 30:2295–2309, Dec 1984.

[54] Mark W. Goodman and Edward Witten. Detectability of certain dark-matter candidates. *Phys. Rev. D*, 31:3059–3063, Jun 1985.

[55] A. Aguilar-Arevalo, D. Amidei, X. Bertou, M. Butner, G. Cancelo, A. Castañeda Vázquez, B.A. Cervantes Vergara, A.E. Chavarria, C.R. Chavez, J.R.T. de Mello Neto, and et al. First direct-detection constraints on ev-scale hidden-photon dark matter with damic at snolab. *Physical Review Letters*, 118(14), Apr 2017.

[56] Michael Crisler, Rouven Essig, Juan Estrada, Guillermo Fernandez, Javier Tiffenberg, Miguel Sofo Haro, Tomer Volansky, and Tien-Tien Yu. Sensei: First direct-detection constraints on sub-gev dark matter from a surface run. *Physical Review Letters*, 121(6), Aug 2018.

[57] Laura Baudis. Wimp dark matter direct-detection searches in noble gases. *Physics of the Dark Universe*, 4:50–59, Sep 2014.

[58] Andrea Caputo, Ciaran A. J. O'Hare, Alexander J. Millar, and Edoardo Vitagliano. Dark photon limits: a cookbook, 2021.

[59] Esra Bulbul, Maxim Markevitch, Adam Foster, Randall K. Smith, Michael Loewenstein, and Scott W. Randall. Detection of an unidentified emission line in the stacked x-ray spectrum of galaxy clusters. *The Astrophysical Journal*, 789(1):13, Jun 2014.

[60] Peter W. Graham, Igor G. Irastorza, Steven K. Lamoreaux, Axel Lindner, and Karl A. van Bibber. Experimental searches for the axion and axion-like particles. *Annual Review of Nuclear and Particle Science*, 65(1):485–514, Oct 2015.

[61] A. Aguilar-Arevalo, D. Amidei, X. Bertou, M. Butner, G. Cancelo, A. Castañeda Vázquez, B.A. Cervantes Vergara, A.E. Chavarria, C.R. Chavez, J.R.T. de Mello Neto, and et al. Search for low-mass wimps in a 0.6 kg day exposure of the damic experiment at snolab. *Physical Review D*, 94(8), Oct 2016.

[62] A. Aguilar-Arevalo, D. Amidei, and others (DAMIC Collaboration). First direct-detection constraints on ev-scale hidden-photon dark matter with damic at snolab. *Phys. Rev. Lett.*, 118:141803, Apr 2017.

[63] A. Aguilar-Arevalo, D. Amidei, D. Baxter, G. Cancelo, B.A. Cervantes Vergara, A.E. Chavarria, E. Darragh-Ford, J.R.T. de Mello Neto, et al. Constraints on light dark matter particles interacting with electrons from damic at snolab. *Physical Review Letters*, 123(18), Oct 2019.

[64] C. J. Bebek, R. A. Coles, et al. CCD research and development at Lawrence Berkeley National Laboratory. In Andrew D. Holland and James W. Beletic, editors, *High Energy, Optical, and Infrared Detectors for Astronomy V*, volume 8453, pages 27 – 42. International Society for Optics and Photonics, SPIE, 2012.

[65] Javier Tiffenberg, Miguel Sofo-Haro, and other. Single-electron and single-photon sensitivity with a silicon skipper ccd. *Phys. Rev. Lett.*, 119:131802, Sep 2017.

[66] Jihn E. Kim. Weak-interaction singlet and strong CP invariance. *Physical Review Letters*, 43(2):103–107, July 1979.

[67] M.A. Shifman, A.I. Vainshtein, and V.I. Zakharov. Can confinement ensure natural cp invariance of strong interactions? *Nuclear Physics B*, 166(3):493–506, 1980.

[68] Patrick Fox, Aaron Pierce, and Scott D. Thomas. Probing a QCD string axion with precision cosmological measurements. 9 2004.

[69] Valerie Domcke and Jan Heisig. Constraints on the reheating temperature from sizable tensor modes. *Physical Review D*, 92(10), Nov 2015.

[70] D. G. Cerdeño and A. M. Green. *Direct detection of WIMPs*, page 347. 2010.

[71] Javier Redondo. Helioscope bounds on hidden sector photons. *Journal of Cosmology and Astroparticle Physics*, 2008(07):008, Jul 2008.

[72] Maxim Pospelov, Adam Ritz, and Mikhail Voloshin. Bosonic super-wimps as kev-scale dark matter. *Physical Review D*, 78(11), Dec 2008.

[73] Naoki Yoshida, Volker Springel, Simon D. M. White, and Giuseppe Tormen. Collisional dark matter and the structure of dark halos. *The Astrophysical Journal*, 535(2):L103–L106, Jun 2000.

[74] Mark Vogelsberger, Jesús Zavala, Francis-Yan Cyr-Racine, et al. Ethos – an effective theory of structure formation: dark matter physics as a possible explanation of the small-scale cdm problems. *Monthly Notices of the Royal Astronomical Society*, 460(2):1399–1416, May 2016.

[75] Roberta Diamanti, Shin'ichiro Ando, Stefano Gariazzo, Olga Mena, and Christoph Weniger. Cold dark matter plus not-so-clumpy dark relics. *Journal of Cosmology and Astroparticle Physics*, 2017(06):008–008, Jun 2017.

[76] S. Agostinelli, J. Allison, and others (Geant4 Collaboration). Geant4—a simulation toolkit. *Nuclear Instruments and Methods in Physics Research Section A: Accelerators, Spectrometers, Detectors and Associated Equipment*, 506(3):250–303, 2003.

[77] `https://ncastell.web.cern.ch/ncastell/pysimdamicm/index.html`. pysimdamicm documentation, last visited 22/06/2021.

[78] Juan Cortabitarte Gutiérrez. Search for dark matter in damic direct search experiments, 7 2020.

[79] Haipeng An, Maxim Pospelov, Josef Pradler, and Adam Ritz. Direct detection constraints on dark photon dark matter. *Physics Letters B*, 747:331–338, Jul 2015.

[80] Yonit Hochberg, Tongyan Lin, and Kathryn M. Zurek. Absorption of light dark matter in semiconductors. *Physical Review D*, 95(2), Jan 2017.

[81] Itay M. Bloch, Rouven Essig, Kohsaku Tobioka, Tomer Volansky, and Tien-Tien Yu. Searching for dark absorption with direct detection experiments. *Journal of High Energy Physics*, 2017(6), Jun 2017.

[82] J.J. Yeh and I. Lindau. Atomic subshell photoionization cross sections and asymmetry parameters: $1 \leq z \leq 103$. *Atomic Data and Nuclear Data Tables*, 32(1):1–155, 1985.

[83] Carsten Schinke, P. Christian Peest, Jan Schmidt, Rolf Brendel, Karsten Bothe, Malte R. Vogt, Ingo Kröger, Stefan Winter, Alfred Schirmacher, Siew Lim, Hieu T. Nguyen, and Daniel MacDonald. Uncertainty analysis for the coefficient of band-to-band absorption of crystalline silicon. *AIP Advances*, 5(6):067168, 2015.

[84] D. E. Aspnes and A. A. Studna. Dielectric functions and optical parameters of si, ge, gap, gaas, gasb, inp, inas, and insb from 1.5 to 6.0 ev. *Phys. Rev. B*, 27:985–1009, Jan 1983.

[85] P. Gondolo and J. Edsjö. Neutralino relic density including coannihilations. *Nuclear Physics B - Proceedings Supplements*, 70(1-3):120–122, Jan 1999.

[86] Kunio Kaneta, Hye-Sung Lee, and Seokhoon Yun. Portal connecting dark photons and axions, 2017.

[87] Paolo Gondolo and Graciela Gelmini. Cosmic abundances of stable particles: Improved analysis. *Nuclear Physics B*, 360(1):145–179, 1991.

# A | Yield equation from scratch

The early universe was radiation-dominated, so its chemical potential was $\mu_\gamma = 0$ and its internal energy $U = \rho V$. By using the Second Law of Thermodynamics:

$$T\,\mathrm{d}S = \mathrm{d}U + P\,\mathrm{d}V - \mu\,\mathrm{d}N\ , \tag{A.1}$$

and the mentioned values of $U$ and $\mu$ in the radiation-dominated universe, we can find how:

$$\mathrm{d}S = \frac{1}{T}\left(\mathrm{d}(\rho V) + P\,\mathrm{d}V\right) = \frac{1}{T}\left(\rho\,\mathrm{d}V + V\,\mathrm{d}\rho + P\,\mathrm{d}V\right) = \frac{1}{T}\left(\mathrm{d}\left[(\rho+P)V\right] - V\,\mathrm{d}P\right)\ . \tag{A.2}$$

Calculating the second derivatives:

$$\frac{\partial S}{\partial V} = \frac{1}{T}\left[\frac{\partial\left[(P+\rho)V\right]}{\partial V} - \frac{V\,\mathrm{d}P}{\partial V}\right] = \frac{1}{T}\left[(\rho+P) - V\frac{\partial P}{\partial V}\right] \Rightarrow \frac{\partial^2 S}{\partial V \partial T} = -\frac{P+\rho}{T^2}\,, \tag{A.3}$$

$$\frac{\partial S}{\partial T} = -\frac{V}{T}\frac{\partial P}{\partial T} \longrightarrow \frac{\partial^2 S}{\partial T \partial V} = -\frac{1}{T}\frac{\partial P}{\partial T}\,, \tag{A.4}$$

and using the equality of second derivatives $\left(\frac{\partial^2 S}{\partial T \partial V} = \frac{\partial^2 S}{\partial V \partial T}\right)$:

$$-\frac{1}{T}\frac{\partial P}{\partial T} = -\frac{\rho+P}{T^2} \longrightarrow \frac{\partial P}{\partial T} = \frac{\rho+P}{T}\,. \tag{A.5}$$

Mixing equation eq. (A.2) and eq. (A.5):

$$\mathrm{d}S = \frac{\mathrm{d}\left[(\rho+P)V\right]}{T} - \frac{V(\rho+P)}{T^2}\,\mathrm{d}T = \mathrm{d}\left[\frac{\rho+P}{T}V\right]\ . \tag{A.6}$$

If we try to find the changes of entropy with time:

$$\begin{aligned}
&\frac{\mathrm{d}S}{\mathrm{d}t} = \frac{\mathrm{d}}{\mathrm{d}t}\left[\frac{\rho+P}{T}V\right] = \frac{V}{T}\left[\frac{\mathrm{d}P}{\mathrm{d}t} + \frac{\mathrm{d}\rho}{\mathrm{d}t}\right] + \frac{P+\rho}{T}\frac{\mathrm{d}V}{\mathrm{d}t} - \frac{(P+\rho)V}{T^2}\frac{\mathrm{d}T}{\mathrm{d}t} = \\
&\left[\frac{V(\rho+P)}{T^2}\frac{\mathrm{d}T}{\mathrm{d}t} - \frac{V(P+\rho)}{T^2}\frac{\mathrm{d}T}{\mathrm{d}t}\right] + \frac{V}{T}\frac{\mathrm{d}\rho}{\mathrm{d}t} + \frac{P+\rho}{T}\frac{\mathrm{d}V}{\mathrm{d}t} = \\
&\frac{V}{T}\frac{\mathrm{d}\rho}{\mathrm{d}t} + \frac{P+\rho}{T}\frac{\mathrm{d}V}{\mathrm{d}t} = \frac{V}{T}\left[\frac{\mathrm{d}\rho}{\mathrm{d}t} + (P+\rho)\frac{\mathrm{d}V}{V\,\mathrm{d}t}\right]\ .
\end{aligned} \tag{A.7}$$

Taking the volume $V$ in terms of the scale factor of the Universe $a$, $V \propto a^{-3}$:

$$\frac{V}{T}\left[\frac{\mathrm{d}\rho}{\mathrm{d}t} + (\rho+P)3\frac{a^{-4}\frac{\mathrm{d}a}{\mathrm{d}t}}{a^{-3}}\right] = \frac{V}{T}\left[\frac{\mathrm{d}\rho}{\mathrm{d}t} + (\rho+P)3H\right] = 0\,. \tag{A.8}$$

The last statement, eq. (A.8) being equal to 0, comes because that equation is exactly the same expression as the continuity equation for the universe.

We have thus found how the entropy is conserved in the thermal bath of the early, radiation-dominated Universe. As the Universe expansion is adiabatic (due to the definition of Universe), entropy must remain constant even beyond equilibrium. We can then define an important quantity, the entropy per comoving volume, i.e. **Entropy density**:

$$s \equiv \frac{S}{V} = \frac{\rho + P}{T} \,. \tag{A.9}$$

We can find a useful expression for the entropy density, computing the density and pressure. We know that the radiation density is that of relativistic bosons:

$$\rho = \frac{g}{(2\pi)^3} \int f(\vec{p}) E(\vec{p}) \, \mathrm{d}^3 p \;, \tag{A.10}$$

with g the degrees of freedom of the gas and $f(\vec{p}) = \frac{1}{e^{\vec{p}/T}-1}$. Assuming an spherical symmetry $E(\vec{p}) \, \mathrm{d}^3 p = 4\pi p^3 \, \mathrm{d}p$, and thus:

$$\rho = \frac{g}{(2\pi)^3} \int_0^\infty \frac{4\pi p^3}{e^{p/T} - 1} \, \mathrm{d}p = \frac{g}{2\pi^2} T^4 \int_0^\infty \frac{x^3}{e^x - 1} \, \mathrm{d}x = \frac{g}{2\pi^2} T^4 \Gamma(4) \zeta(4) = \frac{\pi^2}{30} g T^4 \,. \tag{A.11}$$

Knowing that the pressure in a Bose-Einstein gas is $P = \frac{\rho}{3}$, then:

$$s \equiv \frac{S}{V} = \frac{\rho + P}{T} = \left( \frac{\pi^2}{30} + \frac{\pi^2}{90} \right) g T^3 = \frac{2\pi^2}{45} g T^3 \,. \tag{A.12}$$

Knowing the entropy density in the thermal bath, we can now explore non-equilibrium. First of all, let's start from the Boltzmann equation:

$$\frac{\mathrm{d}n}{\mathrm{d}t} + 3Hn = C[n] \,, \tag{A.13}$$

where $n$ is the number density of any particle, and $C[n]$ is the collision term (all complex physics goes in there, and acts like a cross section for the collision of said $n$ particles). We can try to express the Boltzmann equation in terms of the Yield ($Y = \frac{n}{s}$).

$$\frac{\mathrm{d}}{\mathrm{d}t} \left( \frac{n}{s} \right) = \frac{\mathrm{d}n}{\mathrm{d}t} \frac{1}{s} + n \frac{\mathrm{d}}{\mathrm{d}t} \left( \frac{1}{s} \right) = \frac{1}{s} \frac{\mathrm{d}n}{\mathrm{d}t} - \frac{n}{s^2} \frac{\mathrm{d}s}{\mathrm{d}t} \,. \tag{A.14}$$

Knowing from the entropy conservation calculations that the entropy density is proportional to the scale factor as $s \propto a^{-3}$ :

$$\frac{1}{s} \frac{\mathrm{d}n}{\mathrm{d}t} - \frac{n}{s} \frac{3a^{-4} \frac{\mathrm{d}a}{\mathrm{d}t}}{a^{-3}} = \frac{1}{s} \frac{\mathrm{d}n}{\mathrm{d}t} + 3HY \,. \tag{A.15}$$

All in all:

$$\frac{\mathrm{d}}{\mathrm{d}t}\left(\frac{n}{s}\right) = \frac{\mathrm{d}Y}{\mathrm{d}t} = \frac{1}{s}\frac{\mathrm{d}n}{\mathrm{d}t} + 3HY \longrightarrow \frac{\mathrm{d}n}{\mathrm{d}t} = s\frac{\mathrm{d}Y}{\mathrm{d}t} - 3HsY = s\frac{\mathrm{d}Y}{\mathrm{d}t} - 3Hn\,. \tag{A.16}$$

By comparison with the Boltzmann equation eq. (A.13):

$$C[n] = s\frac{\mathrm{d}Y}{\mathrm{d}t} = s\frac{\mathrm{d}Y}{\mathrm{d}T}\frac{\mathrm{d}T}{\mathrm{d}t} = sT\frac{\mathrm{d}Y}{\mathrm{d}T}\frac{\mathrm{d}T}{T\,\mathrm{d}t} \overset{\left[T\propto a^{-1}\right]}{=\!=} -sT\frac{\mathrm{d}Y}{\mathrm{d}T}\frac{a^{-2}\frac{\mathrm{d}a}{\mathrm{d}t}}{a^{-1}}\,. \tag{A.17}$$

And we finally arrive to equation (14) in [2], which in our calculations is eq. (A.18):

$$-sTH\frac{\mathrm{d}Y_{\gamma'}}{\mathrm{d}T} = \gamma[n_{\gamma'}]\,. \tag{A.18}$$

We can find a useful expression for H working with the Friedmann equation:

$$H^2 - \frac{8}{3}\pi G\rho = -\frac{kc^2}{a^2} = 0\,, \tag{A.19}$$

as $k = 0$ because we have a flat Universe. Hence:

$$H^2 = \frac{\rho}{3}8\pi G = \frac{\pi^2}{90}gT^4\frac{1}{M_{Pl}^2}\,, \tag{A.20}$$

where $M_{Pl} = \frac{1}{\sqrt{8\pi G}} \approx 2.4 \times 10^{18}$ GeV is the reduced Planck Mass.

The problem now comes with the collision term. In general, the collision term is the production rate, minus the annihilation rate. This can include many physical processes depending on the particle we are looking at, but in the case of the Dark Photon production, mediated with the axion, and for Freeze-In production, we just have production of Dark Photons, and a negligible annihilation (pair annihilation of gluons create pairs of Dark Photons). This, in mathematical terms is $\langle\sigma v\rangle n_g^2$, that is the thermal averaged cross section multiplied by the number density of particles, in this case, gluons (squared as they annihilate by pairs). Guided by the calculations in [85] we arrive to the equation (19) in [86]:

$$\gamma[n_{\gamma'}] = \frac{T}{64\pi^4}\int_0^\infty (\sigma v)s^{3/2}K_1\left(\frac{\sqrt{s}}{T}\right)\mathrm{d}s\,. \tag{A.21}$$

To approximate the cross section, we can work with the Feynman diagram:

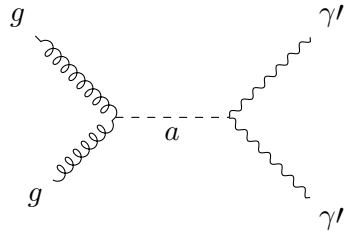

The left vertex will have $G_{agg}$ as coupling, while the right one will be $G_{a\gamma\prime\gamma\prime}$:

$$G_{agg} = \frac{g_s^2}{8\pi^2}\frac{PQ_\Phi}{f_a}\,, \tag{A.22}$$

$$G_{a\gamma\prime\gamma\prime} = \frac{e'^2}{8\pi^2}\frac{PQ_\Phi}{f_a}\left[2N_C D_\psi^2\right]\,. \tag{A.23}$$

With $g_s$ the strong coupling constant, $e'$ the dark coupling constant, $f_a$ the axion decay constant, PQ the dark charge, and $N_C = 3$ the color factor. The cross section can be approximated as:

$$\sigma v \sim \frac{1}{s}|M|^2 \sim \frac{1}{s}|G_{agg}q^2\frac{1}{q^2}G_{a\gamma\prime\gamma\prime}q^2|^2\,, \tag{A.24}$$

where q, the four-momentum of the exchanged particle is $q \sim 2s$, the energy in the center of mass reference frame, and thus:

$$\sigma v \sim 4G_{agg}^2 G_{a\gamma\prime\gamma\prime}^2 s\,. \tag{A.25}$$

Then, going back to eq. (A.21):

$$\gamma[n_{\gamma\prime}] = \frac{T}{64\pi^4}\int_0^\infty 4G_{agg}^2 G_{a\gamma\prime\gamma\prime}^2 s s^{3/2} K_1\left(\frac{\sqrt{s}}{T}\right)\mathrm{d}s\,, \tag{A.26}$$

changing $\frac{\sqrt{s}}{T} = x$, we have:

$$\gamma[n_{\gamma\prime}] = \frac{T}{16\pi^4}\int_0^\infty G_{agg}^2 G_{a\gamma\prime\gamma\prime}^2 x^5 T^5 K_1(x)\,2xT\,\mathrm{d}x =$$

$$= \frac{T^8}{8\pi^4}G_{agg}^2 G_{a\gamma\prime\gamma\prime}^2\int_0^\infty x^6 K_1(x)\,\mathrm{d}x = \frac{48}{\pi^4}G_{agg}^2 G_{a\gamma\prime\gamma\prime}^2 T^8\,. \tag{A.27}$$

Summarizing we can now enter in eq. (A.18) all the three terms eq. (A.12), eq. (A.20) and eq. (A.27), finding:

$$Y_{\gamma\prime}(T=0) = -\int_{T_{RH}}^0 \frac{\gamma[n_{\gamma\prime}]}{SHT}\,\mathrm{d}T = \int_0^{T_{RH}} \frac{\frac{48}{\pi^4}G_{agg}^2 G_{a\gamma\prime\gamma\prime}^2 T^8}{\frac{2\pi^2}{45}gT^3\frac{\pi}{\sqrt{90}}g^{1/2}T^2\frac{1}{M_{Pl}}T}\,\mathrm{d}T = \frac{1080\sqrt{10}}{\pi^7 g^{3/2}}G_{agg}^2 G_{a\gamma\prime\gamma\prime}^2 T_{RH}^3 M_{Pl}\,. \tag{A.28}$$

We can turn this yield into a density parameter, as $\Omega_i = \frac{\rho_i}{\rho_c}$, where $\rho_c = 3H^2 M_{Pl}^2$ is the critical density, and the density can be written as $\rho_i = \frac{M}{V} = mn = msY$. Thus:

$$\Omega_{\gamma\prime}h^2 = \frac{s_0 m_{\gamma\prime}Y_{\gamma\prime}(T=0)}{\frac{\rho_c}{h^2}}\,, \tag{A.29}$$

where the subscript $_0$ means values at the present day: $s_0 = 2889.2\ \mathrm{cm}^{-3}$, $\rho_c = 1.05368\times10^{-5}h^2$ GeV $\mathrm{cm}^{-3}$. We can expand this equation to have all terms, including the Yield from eq. (A.28), and inside it the couplings eqs. (A.22) and (A.23):

$$\Omega_{\gamma'}h^2 = \frac{s_0}{\frac{\rho_c}{h^2}} m_{\gamma'} \frac{1080\sqrt{10}}{\pi^7 g^{3/2}} \left(\frac{g_s^2}{8\pi^2}\frac{PQ_\Phi}{f_a}\right)^2 \left(\frac{e'^2}{8\pi^2}\frac{PQ_\Phi}{f_a}\left[2N_C D_\psi^2\right]\right)^2 T_{RH}^3 M_{Pl}\,. \tag{A.30}$$

Fixing some parameters: the density parameter, so Dark Photons account for all Dark Matter, i.e. $\Omega_{\gamma'}h^2 = 0.12$; $g$ because the degrees of freedom in the very Early Universe (before decoupling of the first species) were close to 100; and $e'$ and $D_\psi$ to typical values for this kind of models; we can get to *Figure 2.3*, relating the mass of the axion to that of the Dark Photon. Up to here, this was the work done in [2].

# B | Minimum mass for Freeze-In

The only calculation between *Figure 2.3* and *Figure 2.4* is the lower bound on the mass of the Dark Photon. It comes from imposing that the reaction rate $r_{\gamma\prime} \equiv \frac{\gamma[n_{\gamma\prime}]}{n^{eq}_{\gamma\prime}}$ is smaller than the rate of expansion (Hubble rate $H$) at the reheating temperature, so we are in the Freeze-In regime, instead of Freeze-Out in which particles interact until the expansion rate is higher than the reaction rate and they cannot keep interacting. Let's track this condition down.

From Boltzmann Statistics we know that the number density at equilibrium is:

$$n^{eq}_{\gamma\prime} = \frac{3\zeta(3)}{\pi^2} T^3 \,, \tag{B.1}$$

where $\zeta$ is the Riemann zeta function, in particular $\zeta(3) = 1.202...$ is the Apéry's constant.

Imposing the reaction rate (remembering eq. (A.27)) smaller than the Hubble rate eq. (A.20) at the reheating temperature, we get:

$$r_{\gamma\prime} \equiv \frac{\gamma[n_{\gamma\prime}]}{n^{eq}_{\gamma\prime}} < H \xrightarrow{T=T_{RH}} \frac{48}{3\pi^2\zeta(3)} G^2_{agg} G^2_{a\gamma\prime\gamma\prime} T^5_{RH} < \frac{\pi}{3\sqrt{10}} g^{1/2} \frac{T^2_{RH}}{M_{Pl}} \,. \tag{B.2}$$

It can be seen how this constraints the reheating temperature to a cubic exponent with the couplings squared, same as happens in eq. (A.30). In fact, mixing both equations, it can be found how:

$$\frac{48}{3\pi^2\zeta(3)} \Omega_{\gamma\prime} h^2 \frac{\frac{\rho_c}{h^2}}{s_0} \frac{\pi^7 g^{3/2}}{1080\sqrt{10}} \frac{1}{m_{\gamma\prime} M_{Pl}} < \frac{\pi}{3\sqrt{10}} g^{1/2} \frac{1}{M_{Pl}} \,, \tag{B.3}$$

so except for the density parameter, the degrees of freedom and the mass of the Dark Photon, the rest are constants. The degrees of freedom for $T = T_{RH}$ are known and constant: $g = 100$, so:

$$m_{\gamma\prime} > \frac{48\pi^4 \frac{\rho_c}{h^2} g}{1080\zeta(3) s_0} \Omega_{\gamma\prime} h^2 \rightarrow m_{\gamma\prime} > 1313.49 \cdot \Omega_{\gamma\prime} h^2 \text{ eV} \,. \tag{B.4}$$

If Dark Photons were the one and only source of Dark Matter in the Universe, it would mean $\Omega_{\gamma\prime} h^2 = 0.12$ and thus $m_{\gamma\prime} > 157.62$ eV. This is an important constraint for Freeze-In model, not remarked by [2], that sets very valuable experimental boundaries.

# C | Freeze-Out calculations

Now let's go for the calculations needed for *figure 2.5*. The first change is the inclusion of the axion relic density, explained in the main text. The other change with respect to *Figure 2.4* is the inclusion of the Freeze-Out model. Freeze-Out model works opposite to the Freeze-In model: In Freeze-Out we start with a large amount of Dark Photons, that are annihilating and turning into gluons until they reach thermal equilibrium. From that point on, the density of Dark Photons becomes fixed until at some point, the interaction is so feeble that it stops (becomes smaller than the expansion rate $H$), leaving the equilibrium value as the relic density for Dark Matter.

So at some temperature $T_{FO}$ the Yield is that of equilibrium, and remains the same up to today:

$$Y_{\gamma\prime}(T_{FO}) = Y^{eq}_{\gamma\prime}(T_{FO}) = \frac{n_{eq}}{s} = Y^0_{\gamma\prime}\,. \tag{C.1}$$

Remembering eq. (B.1) (valid for relativistic particles) and eq. (A.12):

$$Y^0_{\gamma\prime} = \frac{n_{eq}}{s} = \frac{\frac{3\zeta(3)}{\pi^2}T^3_{FO}}{\frac{2\pi^2}{45}gT^3_{FO}} = \frac{135\zeta(3)}{2\pi^4 g}\,. \tag{C.2}$$

It can be seen how in the relativistic Freeze-Out model the Yield is independent on the axion properties, giving it a constant value. It is also independent on the Freeze-Out temperature, so it could happen at any time, but the Freeze-Out temperature is related to $f_a$ so it is restricted to high values. Using eq. (A.29), we find:

$$m_{\gamma\prime} = \frac{\Omega_{\gamma\prime}h^2\frac{\rho_c}{h^2}}{s_0 Y^0_{\gamma\prime}} = 437.83\cdot\Omega_{\gamma\prime}h^2\ \text{eV}\,. \tag{C.3}$$

Let's call it a *magical coincidence*, that this value is exactly $\frac{1}{3}$ of the minimum value for the mass of the Dark Photon in the Freeze-In model.

In the case Dark Photons are not relativistic when they Freeze-Out (necessary for Cold Dark Matter), the number density at equilibrium is:

$$n_{eq} = g\left(\frac{m_{\gamma\prime}T_{FO}}{2\pi}\right)^{3/2} e^{-\frac{m_{\gamma\prime}}{T_{FO}}}\,. \tag{C.4}$$

Therefore, with a similar approach to what was done with Freeze-In eq. (B.2), but keeping the reaction rate equal to $H$ at Freeze-Out temperature:

$$r_{\gamma\prime} \equiv \frac{\gamma[n_{\gamma\prime}]}{n^{eq}_{\gamma\prime}} = H \xrightarrow{T=T_{FO}} \frac{48}{g\pi^4}G^2_{agg}G^2_{a\gamma\prime\gamma\prime}T^8_{FO}\left(\frac{m_{\gamma\prime}T_{FO}}{2\pi}\right)^{-3/2} e^{\frac{m_{\gamma\prime}}{T_{FO}}} = \frac{\pi}{3\sqrt{10}}g^{1/2}\frac{T^2_{FO}}{M_{Pl}}\,. \tag{C.5}$$

Clearing $T_{FO}$, we find:

$$T_{FO} = \frac{-2m_{\gamma\prime}}{9W\left(-\frac{2}{9}m_{\gamma\prime}^{2/3}k^{2/9}\right)}\,, \tag{C.6}$$

where $W()$ is the Lambert W function and $k$ takes all the constant values with it (including in this case $f_a$):

$$k = \frac{81\sqrt{20}}{2\pi^{19/2}}g^{-3/2}\alpha^2(e'D_\psi)^4 f_a^{-4}M_{Pl}\,. \tag{C.7}$$

We can also set another value for $T_{FO}$ with the new Yield:

$$Y_{\gamma\prime}^0 = \frac{n_{eq}}{s} = \frac{45m_{\gamma\prime}^{1/2}e^{-\frac{m_{\gamma\prime}}{T_{FO}}}}{\left(8\pi^5\right)^{1/2}T_{FO}^{3/2}}\,, \tag{C.8}$$

by imposing the density parameter equation eq. (A.29), obtaining:

$$T_{FO} = \frac{-2m_{\gamma\prime}}{3W\left(-\frac{2}{3}\left(\frac{\Omega_{\gamma\prime}h^2\rho_c\left(8\pi^5\right)^{1/2}}{45s_0}\right)^{2/3}\right)}\,. \tag{C.9}$$

It can be clearly seen the correlation between both equations for $T_{FO}$, and it's worth pointing out how in the last case, there is no relation between $T_{FO}$ and $f_a$, but there is with the density parameter $\Omega_{\gamma\prime}h^2$, allowing us to plot this relation, encountering a single slope of permitted values.

All in all, if we have a Freeze-In mechanism we have an open world of opportunities in the parameter space with the axions and Dark Photons together. However, for the relativistic Freeze-Out mechanism, we just have a single value for the mass of the Dark Photons, that is only dependent on its density parameter, almost leaving out the axion properties (there is still a connection between the DP density parameter and the axion density parameter as shown before). In the case of the non-relativistic Freeze-Out, it only leaves open a tiny region with huge masses for both the axions (close to the upper limit in the axion mass) and the Dark Photons (close to the GeV).

All this allows the creation of *Figure 2.5*.

# D | Kinetic mixing Yield

Knowing that the resonant production is incoherent, the evolution for the Dark Photon Yield will be the Boltzmann equation, i.e. eq. (A.18). The only thing that changes from the first model calculations is the collision term, and the inclusion of a correction for later stages in the Early Universe:

$$SHT\frac{\partial Y_{\gamma\prime}}{\partial T} = \Gamma_{\gamma\prime}\frac{\mathrm{d}\ln s}{\mathrm{d}\ln T^3}\,. \tag{D.1}$$

The correction $\frac{\mathrm{d}\ln s}{\mathrm{d}\ln T^3}$ is needed as the effective degrees of freedom for the energy and entropy densities differ as particles decouple from the thermal bath (see [87, 15]).

$\Gamma_{\gamma\prime}$ is the production rate of Dark Photons, which is a sum of all the different contributions, but as mentioned before, for relatively light Dark Photons (1 eV$< m_{\gamma\prime} <$ 1 MeV) the dominant production mechanism is resonance, as electron-positron coalescence is kinematically forbidden. Similar to eq. (A.21), for an $a + b \to \gamma_2 + c$ reaction (as could be for example Compton-like production $e^- + \gamma_1 \to e^- + \gamma_2$):

$$\Gamma_{\gamma\prime} = n_a n_b < \sigma v >= \int \sigma(s) v_{Moel}\,\mathrm{d}n_a\,\mathrm{d}n_b\ , \tag{D.2}$$

where $v_{Moel} = \sqrt{|v_a - v_b|^2 - |v_a \times v_b|^2}$ is the Moeller velocity. Introducing $\sigma = \chi^2\hat{\sigma}$ with the mixing parameter from eq. (2.14), we get the next expression for the Yield:

$$Y_{\gamma\prime} = \sum_{a,b}\int \frac{\hat{\sigma_{ab}} v_{Moel}}{HTs}\frac{\mathrm{d}\ln s}{\mathrm{d}\ln T^3}\frac{\chi_0^2 m_{\gamma\prime}^4}{\left(m_{\gamma\prime}^2 - m_\gamma^2\right)^2 + (\omega D)^2}\,\mathrm{d}T\,\mathrm{d}n_a\,\mathrm{d}n_b\ . \tag{D.3}$$

Expanding around the resonance temperature, $m_\gamma^2(T) = m_{\gamma\prime}^2 + \frac{\mathrm{d}m_\gamma^2}{\mathrm{d}T}(T - T_r) + ...$, we find:

$$Y_{\gamma\prime} \approx \frac{\chi_0^2 m_{\gamma\prime}^4}{HTs}\frac{\mathrm{d}\ln s}{\mathrm{d}\ln T^3}\int \hat{\sigma} v_{Moel}\,\mathrm{d}n_a\,\mathrm{d}n_b\Big|_{T=T_r}\int_0^\infty \frac{\mathrm{d}T}{\frac{\mathrm{d}m_\gamma^2}{\mathrm{d}T}(T - T_r) + (\omega D)^2}\,. \tag{D.4}$$

The temperature integral just gives $\simeq \pi/(\omega D\frac{\mathrm{d}m_\gamma^2}{\mathrm{d}T})$. We can therefore rearrange the integrals over particle three momenta:

$$\int \frac{\hat{\sigma} v_{Moel}}{\omega D}\,\mathrm{d}n_a\,\mathrm{d}n_b\Big|_{m_\gamma = m_{\gamma\prime}} \equiv \int \frac{\Gamma^P}{\omega D}\frac{g_{\gamma_2}}{(2\pi)^3}\,\mathrm{d}^3 p_{\gamma_2} = \int \frac{1}{\omega}\frac{1}{e^{\omega/T} - 1}\frac{g_{\gamma_2}}{(2\pi)^3}\,\mathrm{d}^3 p_{\gamma_2} = \frac{\zeta(2)}{\zeta(3)}\frac{n_\gamma}{T}\,, \tag{D.5}$$

where $\Gamma^P$ is the production rate of photons of energy $\omega$ in the thermal bath at temperature T, and $\Gamma^P(e^{\omega/T}-1)=D$. We have used $m_\gamma = m_{\gamma\prime} \ll T$ and $g_{\gamma_1} = g_{\gamma_2} = 2$ as we are not taking longitudinal photons into account (and we expect that including their effects will not affect our results significantly).

Therefore the final Yield equation is:

$$Y_{\gamma\prime} \simeq \chi_0^2 \frac{\pi\zeta(2)}{\zeta(3)} \frac{m_{\gamma\prime}^2 n_\gamma}{HTs\frac{T}{m_\gamma^2}\frac{\mathrm{d}m_\gamma^2}{\mathrm{d}T}} \frac{\mathrm{d}\ln s}{\mathrm{d}\ln T^3}\bigg|_{T=T_r} \simeq \chi_0^2 \frac{\pi\zeta(2)}{\zeta(3)} \frac{m_{\gamma\prime}^2 Y_\gamma}{HTj(T)} \frac{\mathrm{d}\ln s}{\mathrm{d}\ln T^3}\bigg|_{T=T_r}, \tag{D.6}$$

where $j(T) = \frac{T}{m_\gamma^2}\frac{\mathrm{d}m_\gamma^2}{\mathrm{d}T}$, with the limiting cases $j(T)=3$ for non-relativistic electrons and $j(T)=2$ in the relativistic case.

As for non-relativistic electrons $j(T)=3$, and the number density of photons (relativistic bosons) from Boltzmann Statistics is $n_\gamma = \frac{\zeta(3)}{\pi^2}T^3$, taking into account eq. (A.12), eq. (A.20) and remembering that $T_r \sim 0.2 m_e$ time at which $g \sim 4$, we obtain:

$$Y_{\gamma\prime} \sim \chi_0^2 \frac{m_{\gamma\prime}^2 \zeta(2) 45\sqrt{10} M_{Pl}}{2\pi^4 g^{3/2} (0.2 m_e)^3} \sim \chi_0^2 m_{\gamma\prime}^2 3.38 \times 10^{29}\ \mathrm{GeV}^{-2}. \tag{D.7}$$

We can set this Yield in terms of the density parameter with eq. (A.29), so:

$$\Omega_{\gamma\prime} h^2 = \chi_0^2 m_{\gamma\prime}^3 9.27 \times 10^{37}\ \mathrm{GeV}^{-3}. \tag{D.8}$$

This sets a linear direct correlation depending on how much part of all Dark Matter is accounted by the Dark Photon via kinetic mixing.